

Jet angularities in dijet production in proton–proton and heavy-ion collisions at RHIC

Yang-Ting Chien,^{a,b,c} Oleh Fedkevych,^{a,b,c} Daniel Reichelt,^d Steffen Schumann^e

^a*Physics and Astronomy Department, Georgia State University, Atlanta, GA 30303, USA*

^b*Center for Frontiers in Nuclear Science, Stony Brook University, Stony Brook, NY 11794, USA*

^c*Theory Center, Jefferson Lab, Newport News, Virginia 23606, USA*

^d*Institute for Particle Physics Phenomenology, Department of Physics, Durham University, Durham DH1 3LE, United Kingdom*

^e*Institut für Theoretische Physik, Georg-August-Universität Göttingen, Friedrich-Hund-Platz 1, 37077, Göttingen, Germany*

E-mail: ytchien@gsu.edu, ofedkevych@gsu.edu,
daniel.reichelt@durham.ac.uk, steffen.schumann@phys.uni-goettingen.de

ABSTRACT: We study jet angularities for dijet production at the Relativistic Heavy Ion Collider (RHIC) in proton–proton (pp) and nucleus–nucleus (AA) collisions at 200 GeV nucleon–nucleon center-of-mass collision energy. In particular, we provide NLL resummed predictions for angularity observables of groomed and ungroomed jets produced in pp collisions matched to next-to-leading order QCD calculations resulting in NLO + NLL' accuracy. Our parton-level predictions are corrected for non-perturbative effects, such as hadronization and underlying event, using parton-to-hadron level transfer matrices obtained with the SHERPA event generator. Furthermore, we use the Q-PYTHIA and JEWEL generators to estimate the impact of the interaction between quarks and gluons produced by the parton shower with the dense medium formed in heavy-ion collisions on the considered jet angularities.

Contents

1	Introduction	1
2	Event selections and observable definitions	2
3	All-order resummation at next-to-leading logarithmic accuracy	3
4	Particle-level predictions and non-perturbative corrections	8
5	Estimating medium-interaction effects on jet angularities	19
6	Conclusions	25
A	Connection between transfer matrices and shape functions	27
	References	30

1 Introduction

Jets are collimated sprays of hadronic particles abundantly produced in collider experiments. In a variety of different production processes jets can be instrumented for tests of fundamental properties of the Standard Model (SM) of particle physics as well as for searches of new particles predicted by various SM extensions. As a consequence, within the last decade jet substructure physics has received a lot of attention from both theoretical and experimental communities. Due to the efforts of numerous research groups the field quickly matured and many crucial applications were identified. For example, jet substructure was used in fits of the strong coupling constant [1–5], to constrain parton distribution functions (PDFs) [6–13], to test high-precision perturbative QCD calculations [14, 15], or to search for heavy hadronically decaying resonances predicted by various beyond SM theories [16–19]. Furthermore, jet substructure observables are actively used as input variables for machine learning algorithms, see *e.g.* Refs. [20–22], and for particle tagging purposes [23–29]. Given that the substructure of jets is sensitive to interactions between partons produced in a hard scattering process with the dense medium formed in proton–nucleus (pA) or nucleus–nucleus (AA) collisions, see *e.g.* Refs. [30–39], it provides an important tool to study quark-gluon plasma (QGP) signatures.

Whereas many measurements of jet substructure observables were performed at the Large Hadron Collider (LHC) [40–64], the number of such analyses at the Relativistic Heavy Ion Collider (RHIC) is much smaller, see *e.g.* Refs. [65–68]. However, due to the significantly different collision energies, considerable differences in the jet substructure can be anticipated for jets produced at RHIC with respect to those measured at LHC. In

particular, with the decrease of collision energy and, as a consequence, of the momentum transfer one would expect a much larger impact of non-perturbative physics [69]. This, in turn, challenges the non-perturbative models as implemented in general-purpose Monte Carlo event generators such as PYTHIA [70, 71], HERWIG [72, 73] and SHERPA [74, 75] and may require a dedicated re-tuning of model parameters, see [76, 77]. Therefore, jet substructure studies at RHIC require not only precise first-principles theoretical predictions but also a careful consideration of non-perturbative effects which, as it was demonstrated in Ref. [77], may lead to significant bin-migration processes seriously affecting the shape of jet substructure observables. Given pp collisions are used as a baseline to compare against pA and AA results in QGP searches, a solid understanding of jet substructure physics at RHIC not only in pA and AA but also in pp collisions is needed to facilitate reliable interpretation of experimental measurements.

In this paper we consider a set of jet substructure observables called jet angularities [78–80] which were measured for jets produced in pp collisions at the LHC by the ALICE [15], ATLAS [56] and CMS [14, 53] experiments. Additionally, the ALICE collaboration measured angularities for jets emerging from AA collisions [41]. A closely related set of observables (jet mass and jet shape) was also measured by CDF [81] for $p\bar{p}$ collisions and later by ATLAS, CMS and ALICE in pp [43, 44, 49–54, 56, 57, 59, 60, 62–64] and AA collisions [40, 41, 43, 50, 51, 59, 62], respectively. Additionally, the ALICE collaboration measured the jet mass for jets produced in pA scattering [40].

Important progress has been achieved in recent years on the theoretical description of jet substructure observables. For an overview see [82]. Specifically, high-precision results for jet angularities were presented in Refs. [77, 83–88]. In particular, the NLO + NLL' accurate jet angularity predictions from Refs. [77, 83] were compiled using the resummation plugin to the SHERPA generator framework [89, 90] and hence are largely automated. The main scope of this paper is to provide NLO + NLL' predictions for future measurements of jet angularities in pp collisions at RHIC, which is currently operating the new sPHENIX detector in data-taking mode [91], as well as to estimate the rôle of non-perturbative physics and medium-induced effects through dedicated Monte Carlo simulations.

This paper is organized as follows: in Section 2 we provide definitions of the observables under consideration and briefly discuss the details of our theoretical computations, in Section 3 we present resummed predictions for jet angularities at NLO + NLL' accuracy level, in Section 4 we correct our resummed predictions for non-perturbative effects using parton-to-hadron level transfer matrices as introduced in Ref. [77] and compare the results against predictions from the SHERPA and PYTHIA event generators. Finally, in Section 5 we estimate the impact of medium effects based on simulations with the Q-PYTHIA code [92], derived from the PYTHIA 6 generator [71], as well as JEWEL [93]. Our conclusions and a discussion of possible further steps are presented in Section 6.

2 Event selections and observable definitions

We consider dijet final states produced in pp collisions at $\sqrt{s_{pp}} = 200$ GeV center-of-mass collision energy. We use the FASTJET [94] code to cluster final-state particles into jets

according to the anti- k_t jet algorithm [95] with radius parameter $R_0 = 0.4$ and standard E -scheme recombination, *i.e.* the momenta of particles that get combined are simply added such that the resulting jet momentum is given by the sum of its constituents' momenta. We require at least two jets that satisfy

$$p_{T,j_1} > 30 \text{ GeV}, \quad p_{T,j_2} > 20 \text{ GeV} \quad \text{and} \quad |y_{j_1,j_2}| < 0.7, \quad (2.1)$$

which is in accordance with the RHIC detector acceptance characteristics and the sPHENIX beam use proposal [91]. Through the staggered transverse momentum cuts we avoid perturbative instabilities appearing for exactly balanced back-to-back dijet kinematics, see Ref. [96] for a detailed discussion. In each selected event, we consider the two leading transverse momentum jets, and for each jet individually evaluate the angularity observables [78–80] defined as

$$\lambda_\alpha^\kappa = \sum_{i \in \text{jet}} \left(\frac{p_{T,i}}{\sum_{j \in \text{jet}} p_{T,j}} \right)^\kappa \left(\frac{\Delta_i}{R_0} \right)^\alpha \equiv \sum_{i \in \text{jet}} z_i^\kappa \left(\frac{\Delta_i}{R_0} \right)^\alpha, \quad (2.2)$$

where

$$\Delta_i = \sqrt{(y_i - y_{\text{jet}})^2 + (\phi_i - \phi_{\text{jet}})^2}, \quad (2.3)$$

is the standard Euclidean azimuth-rapidity distance between particle i and the jet axis. The concept of infrared and collinear (IRC) safety requires $\kappa = 1$ and $\alpha > 0$. Therefore, we limit ourselves to three commonly studied cases: $\lambda_{1/2}^1$ (Les Houches angularity or LHA), λ_1^1 (Jet Width) and λ_2^1 (Jet Thrust) [14, 80, 97]. Also, in order to keep our notation simple, in the rest of the paper we omit the subscript κ assuming $\kappa = 1$. Ultimately, we consider the sum of the distributions individually determined for the two leading jets as described above.

Angularities with $\alpha \leq 1$ are sensitive to recoil against soft emissions [98, 99], leading to a rather complicated resummation structure. To avoid the complication caused by recoil effects, for $\lambda_{1/2}$ and λ_1 we evaluate the distance measure in Eq. (2.3) with respect to the jet axis obtained by reclustering the jet constituents with the anti- k_t algorithm but using the Winner-Take-All (WTA) recombination scheme [100].

We also consider groomed jets where as a groomer we use the **SoftDrop** algorithm with parameters $z_{\text{cut}} = 0.2$ and $\beta = 0$ [101, 102] and the Cambridge–Aachen (C/A) algorithm [103, 104] for jet reclustering. To this end we use the **fjcontrib** implementation of **SoftDrop** in the FASTJET package. The angularity is then computed on the resulting groomed jet, *i.e.* both sums in Eq. (2.2) are restricted to the particles that survived the grooming. Also for groomed jets we adopt the WTA prescription for angularities with $\alpha \leq 1$.

In practice, we use the RIVET framework [105, 106] to perform the Monte Carlo analysis and use Matplotlib [107] for plotting.

3 All-order resummation at next-to-leading logarithmic accuracy

To perform NLL resummation for jet angularities we use the SHERPA implementation of the CAESAR resummation formalism [98, 108], first presented in [89]. This framework has been

employed to obtain resummed predictions for **SoftDrop** thrust [109] and multijet resolution scales [90] in electron–positron collisions, as well as NLO + NLL' predictions for **SoftDrop** groomed hadronic event shapes [110], for jet angularities in dijet and Z +jet production at the LHC [24, 77, 83] and, recently, for plain and groomed event shapes in neutral-current deep inelastic scattering [111–113], as well as event-shape observables in hadronic Higgs-boson decays [114].

For an applicable jet-substructure observable, the all-order cumulative cross section for observable values up to v , with $L = -\ln(v)$, can be written as a sum over partonic channels δ :

$$\begin{aligned} \Sigma_{\text{res}}(v) &= \sum_{\delta} \Sigma_{\text{res}}^{\delta}(v), \text{ with} \\ \Sigma_{\text{res}}^{\delta}(v) &= \int d\mathcal{B}_{\delta} \frac{d\sigma_{\delta}}{d\mathcal{B}_{\delta}} \exp \left[- \sum_{l \in \delta} R_l^{\mathcal{B}_{\delta}}(L) \right] \mathcal{S}^{\mathcal{B}_{\delta}}(L) \mathcal{F}^{\mathcal{B}_{\delta}}(L) \mathcal{H}^{\delta}(\mathcal{B}_{\delta}), \end{aligned} \quad (3.1)$$

where $\frac{d\sigma_{\delta}}{d\mathcal{B}_{\delta}}$ is the fully differential Born cross section for the subprocess δ and \mathcal{H} implements constraints on the Born phase space \mathcal{B} . The label \mathcal{F} represents the multiple emission function which, for additive observables such as the angularities considered in this paper, is simply given by $\mathcal{F}(L) = e^{-\gamma_E R'} / \Gamma(1 + R')$, with $R'(L) = \partial R / \partial L$ and $R(L) = \sum_{l \in \delta} R_l(L)$. The soft function \mathcal{S} implements the non-trivial aspects of color evolution. In our notation this includes the effect of non-global logarithms [115]. Since the relevant functions depend on the jet radius only, we here can use the expressions extracted numerically in the leading-color approximation from [77], based on the code from [83]. The collinear radiators R_l for the hard legs l are summarized in [98] for a general global observable V scaling for the emission of a soft-gluon of relative transverse momentum $k_t^{(l)}$, rapidity $\eta^{(l)}$ and azimuthal angle $\phi^{(l)}$ with respect to leg l as

$$V(k) = \left(\frac{k_t^{(l)}}{\mu_Q} \right)^a e^{-b_l \eta^{(l)}} d_l(\mu_Q) g_l(\phi^{(l)}), \quad (3.2)$$

while here we have to take into account the modifications from [83, 116] to account for the phase-space restrictions implied by the finite jet radius. For the jet angularities defined by Eq. (2.2) it holds [83]

$$a = 1, \quad b_l = b = \alpha - 1, \quad g_l d_l = \left(\frac{2 \cosh \eta_{\text{jet}}}{R_0} \right)^{\alpha-1} \frac{\mu_Q}{p_{T,\text{jet}} R_0}. \quad (3.3)$$

Here, we denote the transverse momentum and rapidity (noting that the resummation is performed around configurations corresponding to massless jets) by η_{jet} , $p_{T,\text{jet}}$. We choose $\mu_Q = p_{T,\text{jet}} R_0$, simplifying the last term in $g_l d_l$ to unity.

Generalized expressions for the radiator functions, that we use here when considering **SoftDrop** groomed final states with general parameters z_{cut} and β , have been presented in [110]. As discussed in [77, 83] our resummation is strictly valid in the limit of small z_{cut} , *i.e.* $\lambda_{\alpha} \ll z_{\text{cut}} \ll 1$. However, for $\beta = 0$ finite- z_{cut} corrections are already present at the (leading) single-logarithmic accuracy [117], and have been found to have a negligible effect

in practice [101] at least for $z_{\text{cut}} = 0.1$. We will assume that similar statements can be made for $z_{\text{cut}} = 0.2$ and do not include any related corrections.

The CAESAR resummation plugin to SHERPA hooks into the event generation framework, facilitating the process management, and providing access to the COMIX matrix-element generator [118], as well as phase-space integration and event-analysis functionalities. The SHERPA framework is also used to compile all the required higher-order tree-level and one-loop calculations. The plugin implements the building blocks of the CAESAR master formula Eq. (3.1), along with the necessary expansion in the strong coupling constant α_s used in the matching with fixed-order calculations. All elements are evaluated fully differentially for each Born-level configuration \mathcal{B}_δ of a given flavor and momentum configuration.

The treatment of the kinematic endpoint is implemented in the same way as in Ref. [110] by shifting the relevant logarithms and adding power-suppressed terms to achieve a cumulative distribution that approaches one at the kinematic endpoint and has a smooth derivative approaching zero. In particular, we introduce the additional parameters p, x_L, v_{max} and modify all logarithms according to

$$\ln\left(\frac{x_L}{v}\right) \rightarrow \frac{1}{p} \ln\left[\left(\frac{x_L}{v}\right)^p - \left(\frac{x_L}{v_{\text{max}}}\right)^p + 1\right] = L. \quad (3.4)$$

Here we set v_{max} to the numerically determined endpoint of the observable distribution evaluated at NLO, and by default use $p = 1$. We set $x_L = 1$, while a variation of this parameter can be used to assess uncertainties of the resummed calculation. Note that $x_L \neq 1$ introduces additional NLL terms that need to be subtracted.

To adequately describe intermediate and large angularity observable values, the resummed calculation needs to be matched to an appropriate fixed-order calculation. We use the COMIX matrix-element generator shipped with SHERPA to perform an NLO calculation for the dijet final state. In order to capture the next-order corrections for jet shapes like the angularities, it is sufficient to perform an NLO calculation for the 3-parton final state, with a small cut-off $\lambda_\alpha^{\text{min}}$ in the observable to regularize the divergences from double soft and triple collinear splittings. In practice we choose $\lambda_\alpha^{\text{min}}$ to be smaller than the smallest bin edge considered, and enforce the physical condition $\Sigma(0) = 0$ in our matching prescription. Note that this means that our calculation technically becomes observable specific and we perform separate calculations for angularities measured on the more central and more forward of the two leading jets, while keeping the phase space for radiation in the other jet unrestricted. We use the SHERPA implementation of the Catani–Seymour dipole subtraction scheme [119] and the interfaces to the RECOLA [120, 121] and OPENLOOPS [122] one-loop amplitude generators.

To combine our NLL results with the fixed-order calculation, we perform a multiplicative matching, separately for quark and gluon jets in order to ensure an effective extraction of the C_1 coefficients necessary to achieve NLO+NLL' accuracy. While several more sophisticated jet-flavor algorithms have appeared since then [123–127], we stick with the iterative application of [128] introduced in [83] since it is sufficient for our purpose. We stress again that we can perform all required fixed-order calculations efficiently with the generic tools available in SHERPA to the numerical accuracy necessary for an effective matching. After

matching, we stack the two distributions for the central and forward jet, to obtain a prediction for the summed distribution that would be obtained by filling a histogram with the values of both the leading jets for each event.

As parton density distributions we use the NNLO PDF4LHC21_40_pdfas set [129] with $\alpha_s(M_Z) = 0.118$, accessed via the LHAPDF library [130]. The central values for the perturbative factorization (μ_F) and renormalization (μ_R) scales entering the calculation are set to

$$\mu_F = \mu_R = H_T/2. \quad (3.5)$$

To estimate the perturbative uncertainties of our predictions, we perform on-the-fly [131] 7-point variations using

$$\left\{ \left(\frac{1}{2}\mu_R, \frac{1}{2}\mu_F \right), \left(\frac{1}{2}\mu_R, \mu_F \right), \left(\mu_R, \frac{1}{2}\mu_F \right), \left(\mu_R, \mu_F \right), \left(\mu_R, 2\mu_F \right), \left(2\mu_R, \mu_F \right), \left(2\mu_R, 2\mu_F \right) \right\}, \quad (3.6)$$

as well as an independent variation of the parameter x_L introduced in Eq. (3.4), corresponding to $x_L = 1/2$ and $x_L = 2$.

In Fig. 1 we present resummed predictions, without any non-perturbative correction dubbed parton level (PL), for the jet-angularity observables in proton–proton collisions at $\sqrt{s_{pp}} = 200$ GeV. In general, larger values of the angularities correspond to jets with increased internal activity, either in the form of more or harder constituents. On the other hand, the $\lambda_\alpha \rightarrow 0$ limit corresponds to jets with no or only soft and/or collinear radiation. However, due to the different scaling of the observables, equal values of the angularities across our choices for α probe different overall levels of softness. For this reason, $\lambda_{1/2}$ showcases the typical behavior of a jet shape, with a Sudakov peak produced by logarithmic terms at all orders that dampen the rise present in the leading-order contributions when $\lambda \rightarrow 0$. The region to the left of the peak is fully resolved and we can follow the suppression of events at very small $\lambda_{1/2}$ until the height of the first bin is effectively 0. This picture is much less clear for λ_1 , since the same values of λ_1 correspond to harder configurations, so the peak is at smaller values and we can only observe the maximum of the distribution in the bin corresponding to the second smallest λ_1 range. Finally, for λ_2 this becomes even stronger and we do not observe any peak structure given this binning choice. Of course the resummed distribution still approaches 0 at $\lambda = 0$, however, the maximum would only be in the first bin, such that we can not resolve the Sudakov peak structure. When comparing the ungroomed distributions with the corresponding groomed ones, the latter, as expected, are shifted towards smaller angularity values. **SoftDrop** grooming eliminates part of the jet constituents, thus sharpens the jet profile. While these differences are of course to some extent an artifact of our chosen binning, this binning is motivated by the resolution achieved by the LHC experiments, in particular the measurement in [14], where a similar effect when changing α is observed. While from a theoretical point of view it might be interesting to study the deep IR limit, see for example [83], we here stick to predictions in a setting that should roughly be achievable in an actual experiment at RHIC.

We only find moderate effects from the matching of resummation and fixed-order calculations at LO and NLO. When going from the pure NLL results to the leading order

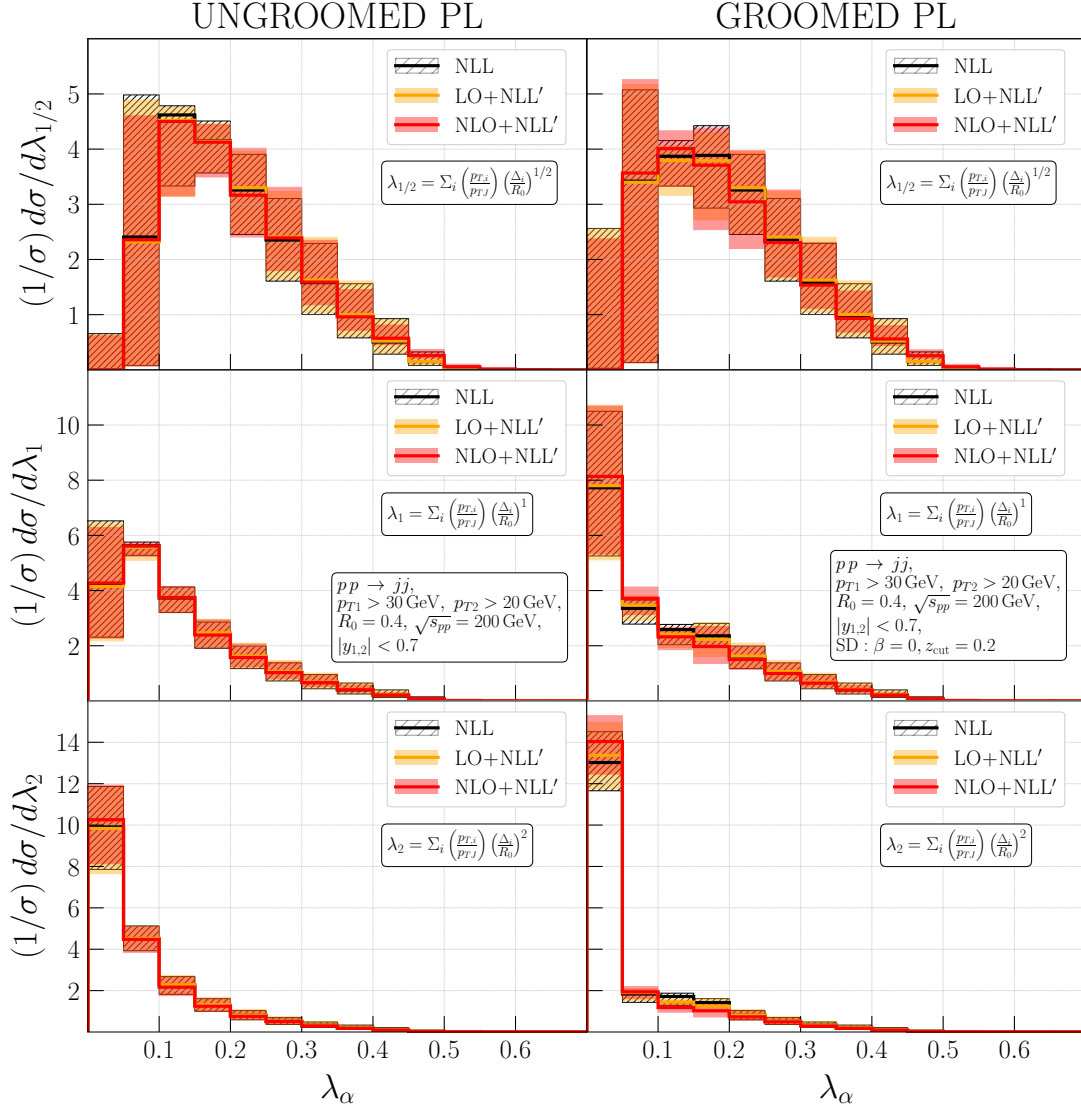


Figure 1: Normalized parton-level resummed predictions for the $\lambda_{1/2}$, λ_1 , λ_2 angularity distributions (top to bottom) without and with **SoftDrop** grooming (left and right). We illustrate the effect of matching to the fixed-order calculation by showing the pure NLL result (red) compared to the leading-order matched one (orange) and our final NLO + NLL' accurate matched result (black).

accurate LO + NLL', all distributions are slightly shifted towards larger values of the respective angularities. This is most visible in the groomed case, where for $\alpha = 1, 2$ the height of the first bin is visibly reduced. For $\alpha = 1/2$ the first bin is already suppressed, but we still observe a small shift in the peak position. The changes in the ungroomed distributions are less prominent but qualitatively consistent with the above observations. The effect in some cases becomes stronger after including NLO corrections, which are small in all cases.

However, the impact of including fixed-order corrections, even at LO, on the central

value is dwarfed by the remaining uncertainty. These are estimated by the envelope of 7-point variations of the renormalization and factorization scales μ_R , μ_F , and variations of the resummation scale factor x_L introduced in Eq. (3.4). The widths of the uncertainty bands are dominated by the x_L variations, corresponding to setting $x_L = 2$ and $x_L = 1/2$. We hence observe at best a small impact of the matching to higher orders on the total uncertainty, though in some cases a reduction is visible. In general, the uncertainties are moderate in size. Exceptionally, they are very large for the first bin including $\lambda = 0$, and the first few bins, towards smaller values from the peak position, for the Les Houches angularity $\lambda_{1/2}$. The main effect of the x_L variation is a shift of the distribution towards smaller/larger observable values. Hence, the bins in the vicinity of the distributions peak are most affected by these shifts. Given that the angularity distributions typically fall off very sharply to the left of the maximum, this results in quite significant uncertainties in this region.

4 Particle-level predictions and non-perturbative corrections

To derive actual particle-level predictions, *i.e.* for final states of detectable hadrons, we perform corresponding Monte Carlo simulations with SHERPA and PYTHIA [70], thereby accounting for non-perturbative effects such as hadronization and the underlying event (UE) contribution [132, 133].

As demonstrated in a variety of works [134–138], non-perturbative corrections to IRC-safe jet-substructure observables have a power-suppressed form which allows one to consider them as sub-leading corrections for large and moderate jet- p_T values, see, for example, Ref. [77]. Nevertheless, as the jet’s transverse momentum decreases, one would anticipate that non-perturbative corrections leave a more pronounced impact on the jet substructure. Moreover, given that collision energies at RHIC are much smaller compared to the LHC, possibly re-tuning of the parameters of UE and hadronization models might be needed, to ensure that different physics aspects relevant at LHC and RHIC are properly taken into account.

Given there is no unique procedure how to incorporate non-perturbative effects into resummed calculations, special attention needs to be paid to the choice of the correction scheme when comparing first-principles theoretical predictions against jet-substructure measurements of low- p_T jets. We here correct our resummed predictions for hadronization and the underlying event using parton-to-hadron level transfer matrices derived from dedicated SHERPA simulations as introduced in Ref. [77].

Hadron-level simulations with SHERPA and PYTHIA

For SHERPA we use version 3.0.0 β , considering inclusive dijet production based on its implementation of the MC@NLO formalism [139], dubbed SHERPA MC@NLO in what follows. The NLO QCD matrix elements for two-jet production get matched with the SHERPA Catani–Seymour dipole shower [140]. The involved QCD one-loop amplitudes we obtain from the OPENLOOPS library which uses the COLLIER package [141] for the evaluation of tensor and scalar integrals.

As for the resummed calculation we employ the NNLO PDF4LHC21_40_pdfas set and $\alpha_s(M_Z) = 0.118$. The central values for the perturbative scales are set to

$$\mu_F = \mu_R = \mu_Q = H_T/2. \quad (4.1)$$

Scale uncertainties get estimated through 7-point variations of μ_F and μ_R , see Eq. (3.6), both in the matrix elements and the parton shower, while we keep the parton-shower starting scale (μ_Q) fixed [131]. The SHERPA UE simulation [75] is based on an implementation of the Sjöstrand–Zijl multiple-parton interaction (MPI) model [142]. To account for the parton-to-hadron transition we use the SHERPA cluster fragmentation [143]. Here we include an estimate of the hadronization parameter uncertainty, based on replica tunes, first presented in [111, 144]. To this end, besides the nominal default tune, we run SHERPA with the hadronization parameters set according to 7 replica tunes, thereby using the central choice for μ_R and μ_F . Each of the runs produces an alternative distribution that we treat on an equal footing with the scale variations and use the envelope of all variations as an estimate for the total uncertainty.

In Fig. 2 we present the predictions from SHERPA for simulations at parton level, *i.e.* with hadronization and UE disabled, and at hadron level, where both effects are taken into account. The general features of the distributions parallel the observations for the resummed results in Fig. 1. We note that the parton-level distributions show a significant peak in the first bin, caused by the finite parton-shower cutoff, that effectively prevents particle production below a certain hardness scale of $\mathcal{O}(1 \text{ GeV})$. This leads to an overpopulation of the first bin from jets with no resolvable emission above this cutoff. Within the factorized MC approach, the hadronization model is responsible for re-distributing these jets towards non-vanishing angularities. On the other hand, the resummed predictions shown earlier do not feature such cutoff, as all integrals are formally taken across the Landau pole. Hence, it is evident that a simple ratio of the bin entries at hadron and parton level, at least close to the shower cutoff, does not suffice to correct resummed calculations and we therefore have to resort to more sophisticated approaches. We here make use of a multi-differential transfer-matrix technique introduced in [77], detailed below.

Even when ignoring shower-cutoff effects, the impact of hadronization and UE on the angularity distributions is quite significant, resulting in a change of the peak position for most cases. In particular the Les Houches angularity $\lambda_{1/2}$ is known to be very sensitive to non-perturbative effects, see, *e.g.* Refs. [77, 83]. A notable exception appears to be the groomed $\alpha = 2$ case, where parton- and hadron-level predictions from SHERPA seem to largely agree. However, as explained above, for $\alpha = 2$ most of the jets with deeply soft radiation end up in the first bin, such that we do not resolve them very well for λ_2 . In general, **SoftDrop** grooming significantly ameliorates the impact of non-perturbative effects on the angularity distributions.

To obtain alternative hadron-level predictions we ran further simulations with PYTHIA using version 8.310 [70]. To this end, we simulate inclusive dijet production at the leading order using the PYTHIA 8 default parton shower [145, 146]. Given the drastic difference of proton–proton collision energy between RHIC and LHC might necessitate adjustments of the non-perturbative model parameters, we here employ a dedicated tune of PYTHIA

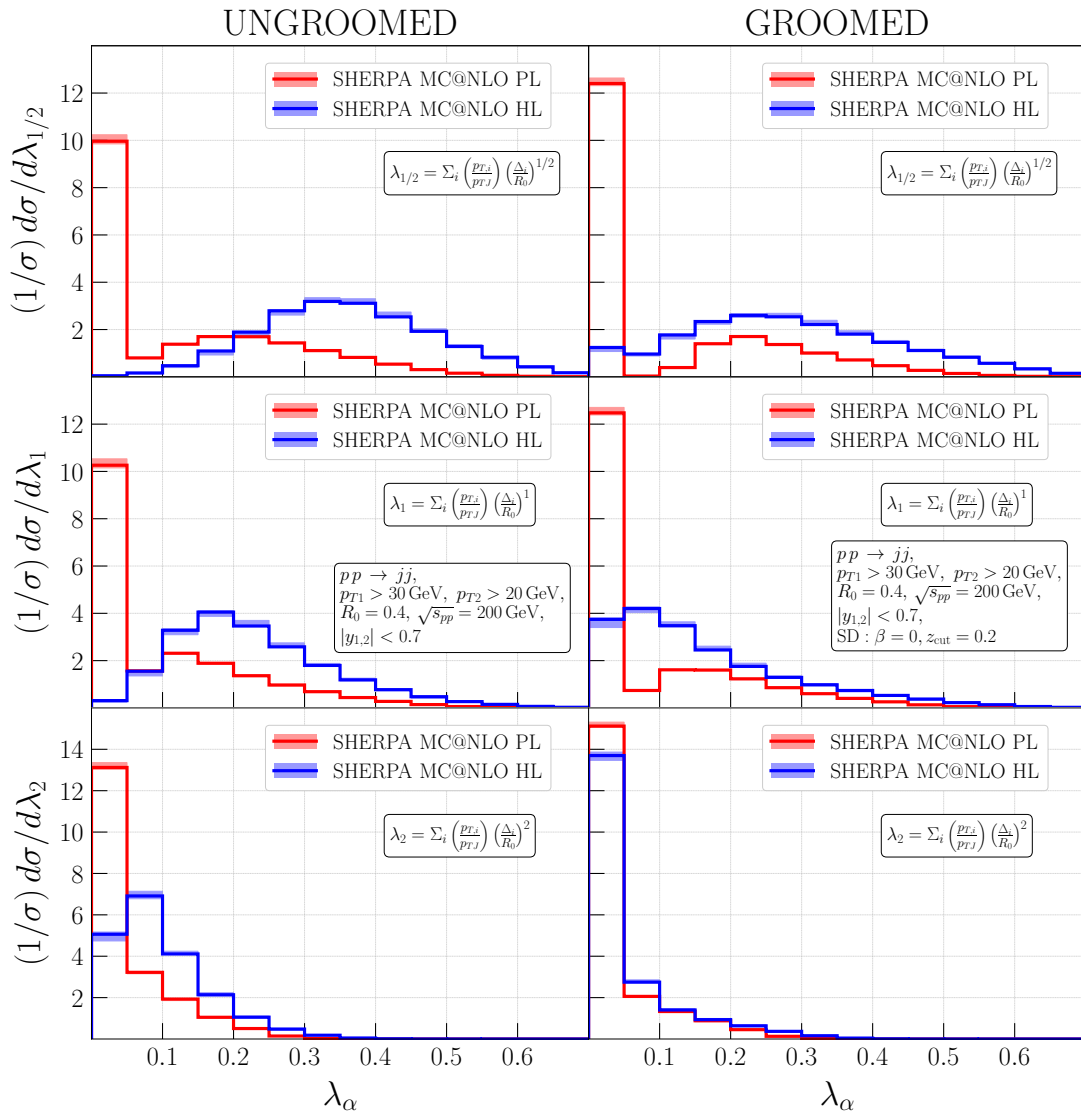


Figure 2: Normalized parton- and hadron-level Monte Carlo predictions obtained with SHERPA for the $\lambda_{1/2}$, λ_1 , λ_2 angularity distributions (top to bottom) without and with SoftDrop grooming (left and right).

optimized for the description of RHIC data, referred to as *Detroit tune* [76]. For reference, we also derived predictions based on the PYTHIA 8 default, the so-called *Monash tune* [147].

In Fig. 3 we present a comparison of hadron-level predictions obtained with PYTHIA based on the Detroit and Monash tunes, as well as those from SHERPA using its default tune. In general, the particle-level results from the two generators agree quite well regarding the shapes of the plain and the soft-drop groomed angularity distributions. However, the PYTHIA results for both tunes are slightly shifted towards larger angularity values, corresponding to a broader jet-constituent distribution. This effect is somewhat more pronounced for the Monash tune, PYTHIA’s default. The dedicated Detroit tune appears to

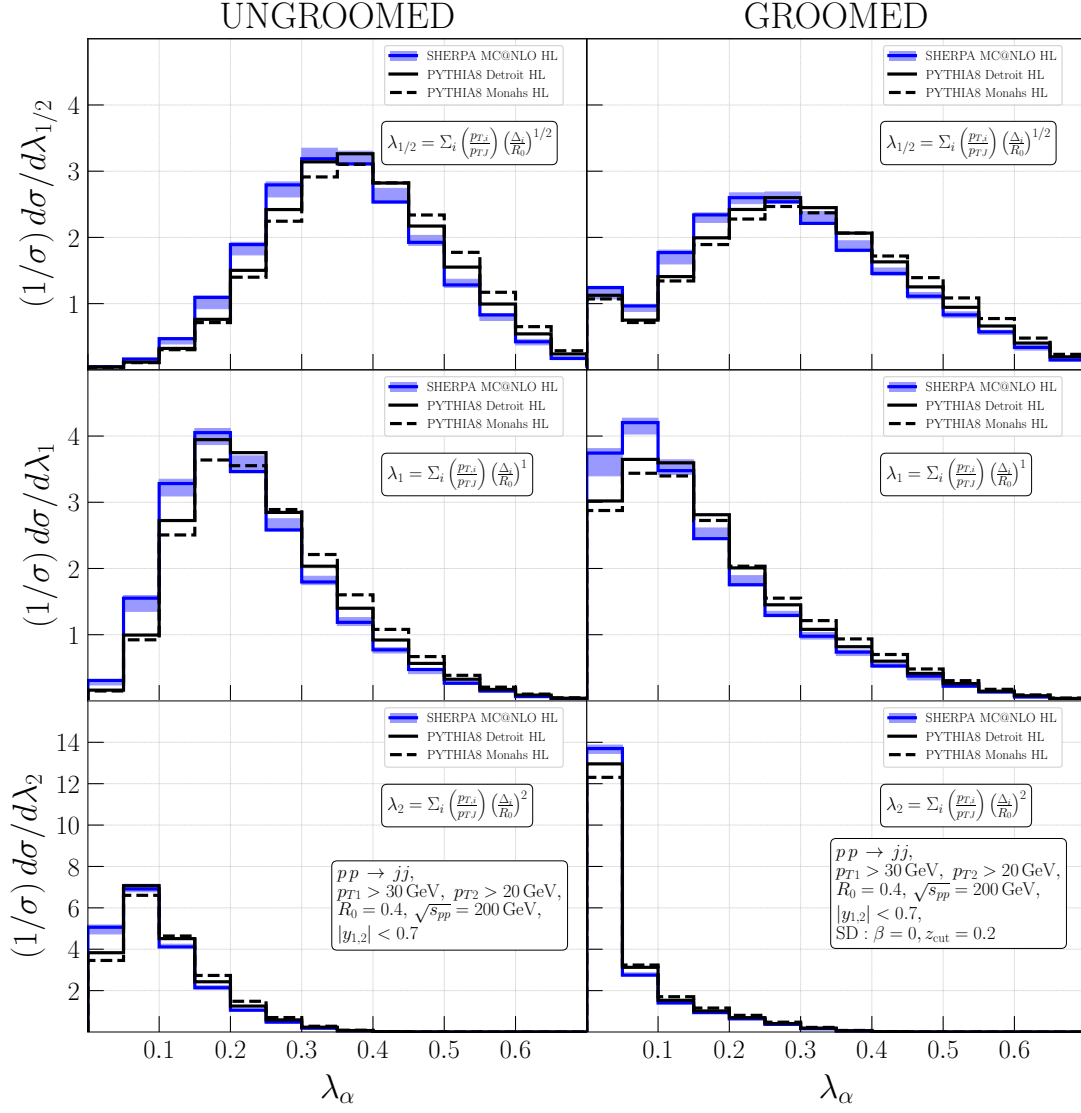


Figure 3: Comparison of hadron-level predictions for the ungroomed and groomed angularity observables $\lambda_{1/2}$, λ_1 and λ_2 from SHERPA MC@NLO (default tune) and PYTHIA 8 results obtained for the “Detroit” tune [76] and the default Monash 2013 tune [147].

produce results in-between the SHERPA MC@NLO and the PYTHIA Monash-tune predictions. The dominant difference between the two PYTHIA tunes consists in the parameter settings affecting the UE activity, see Ref. [76] for details. Given the significantly lower proton-beam energy at RHIC in comparison to the LHC, the average number of secondary scatterings per proton–proton collision at RHIC is much smaller. This is illustrated in Fig. 4, where we show the distribution of MPI scatters associated with a dijet-production hard process, using the event selection criteria listed in Sec. 2, for $\sqrt{s_{pp}} = 200$ GeV and $\sqrt{s_{pp}} = 13$ TeV, respectively. For the LHC setup we show predictions based on the Monash tune, the PYTHIA 8 default in particular for LHC simulations. The distribution is rather

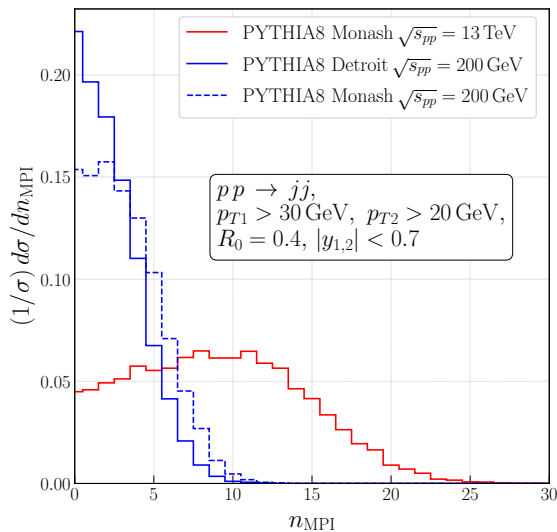


Figure 4: Number of secondary scatterings per proton–proton collision at RHIC (blue lines) and LHC (red line) as predicted by the PYTHIA 8 event generator. For the LHC case we show predictions based on the default Monash tune. For the RHIC scenario we present results both for the Detroit (solid) and the Monash (dashed) tune.

broad and peaks around $n_{\text{MPI}} \approx 10$. In contrast, at RHIC energies the distribution based on the Monash-tune parameters has its maximum at $n_{\text{MPI}} = 2$ and is rather narrow. Considering the Detroit tune, the distribution peaks at $n_{\text{MPI}} = 0$ and is quickly falling. Accordingly, the majority of events has either no or only 1-2 associated secondary scatterings. These differences in MPI activity for the two tunes explain the shifts in the angularity distributions observed in Fig. 3. In conclusion, for the here considered event-selection criteria most of the hadronic collision energy at RHIC is deposited in the hard scattering, while the impact of the UE is significantly reduced compared to the LHC. As a consequence, non-perturbative corrections that affect jet-substructure observables at RHIC are largely dominated by hadronization effects. Accordingly, studies of jet angularities sensitive to non-perturbative corrections, as in particular $\lambda_{1/2}$, provide stringent tests for hadronization models as implemented in general-purpose MC generators.

The transfer-matrix approach to non-perturbative corrections

To account for the alteration of the derived resummed jet angularity distributions due to non-perturbative corrections we employ parton-to-hadron level transfer matrices as introduced in Ref. [77]. This quite general approach is applicable to an arbitrary set of observables, measured in a multi-differential way. In general, it aims to keep track both of the migration in event kinematics, used to define the fiducial phase space, that get partially integrated over, as well as changes in the actual observable of interest, *i.e.* in the here considered case the angularity variable.

We consider a generic scattering process which results in a partonic configuration \mathcal{P} .

Through NP effects the set of parton momenta gets mapped onto a hadron-level configuration $\mathcal{H}(\mathcal{P})$. The map \mathcal{H} thereby accounts for hadronization and UE corrections. It could be derived from field-theoretical considerations (see for example Refs. [148, 149] for recent work on **SoftDrop** observables) or it can be extracted from parton-shower simulations interfaced to a model of NP phenomena. For a given configuration \mathcal{P} or $\mathcal{H}(\mathcal{P})$, we then measure a set of m observables, $\vec{V}(\mathcal{P})$ or $\vec{V}(\mathcal{H}(\mathcal{P}))$.¹ We define the transfer operator as the conditional probability to measure a set of observables \vec{v}_h at hadron level on $\mathcal{H}(\mathcal{P})$, given that the parton-level observables were \vec{v}_p :

$$\mathcal{T}(\vec{v}_h|\vec{v}_p) = \frac{\int d\mathcal{P} \frac{d\sigma}{d\mathcal{P}} \delta^{(m)}(\vec{v}_p - \vec{V}(\mathcal{P})) \delta^{(n)}(\vec{v}_h - \vec{V}(\mathcal{H}(\mathcal{P})))}{\int d\mathcal{P} \frac{d\sigma}{d\mathcal{P}} \delta^{(m)}(\vec{v}_p - \vec{V}(\mathcal{P}))}. \quad (4.2)$$

This way, the multi-differential distribution for the set of hadron-level observables \vec{v}_h can be written as

$$\frac{d^m \sigma^{\text{HL}}}{dv_{h,1} \dots dv_{h,m}} = \int d^m \vec{v}_p \mathcal{T}(\vec{v}_h|\vec{v}_p) \frac{d^m \sigma^{\text{PL}}}{dv_{p,1} \dots dv_{p,m}}. \quad (4.3)$$

When working with binned distributions, one obtains binned cross sections by integrating the multi-differential distribution over hypercubes in the observables' space. At parton level the cross section in any given hyper-bin p can be written as

$$\Delta\sigma_p^{\text{PL}} = \int d\mathcal{P} \frac{d\sigma}{d\mathcal{P}} \Theta_p(\mathcal{P}), \quad (4.4)$$

where

$$\Theta_p(\mathcal{P}) = \prod_{i=1}^m \theta(V_i(\mathcal{P}) - v_{p,i}^{\text{min}}) \theta(v_{p,i}^{\text{max}} - V_i(\mathcal{P})). \quad (4.5)$$

When considering a binned distribution at hadron level, the transfer operator from parton-level bin p to a given hadron-level bin h becomes a matrix of the form

$$\mathcal{T}_{hp} = \frac{\int d\mathcal{P} \frac{d\sigma}{d\mathcal{P}} \Theta_p(\mathcal{P}) \Theta_h(\mathcal{H}(\mathcal{P}))}{\int d\mathcal{P} \frac{d\sigma}{d\mathcal{P}} \Theta_p(\mathcal{P})}, \quad (4.6)$$

with

$$\Theta_h(\mathcal{H}(\mathcal{P})) = \prod_{i=1}^m \theta(V_i(\mathcal{H}(\mathcal{P})) - v_{h,i}^{\text{min}}) \theta(v_{h,i}^{\text{max}} - V_i(\mathcal{H}(\mathcal{P}))). \quad (4.7)$$

Consequently, the final hadron-level distribution in the hyper-bin h is obtained by the weighted sum of all parton-level contributions

$$\Delta\sigma_h^{\text{HL}} = \sum_p \mathcal{T}_{hp} \Delta\sigma_p^{\text{PL}}. \quad (4.8)$$

¹For simplicity we here have chosen the same set of observables \vec{V} on the parton- and hadron-level configurations which, however, is not strictly necessary.

The elements of the transfer matrices appearing in Eq. (4.8) can easily be extracted from a multi-purpose generator in a single run, provided that individual events are accessible at different stages of their evolution in the simulation process. Note however that, while parton shower and hadronization are treated in a factorized form in all multi-purpose event generators [132], this is not necessarily the case for the UE. In particular, PYTHIA 8 [150] makes use of an interleaved evolution of the initial-state shower and the secondary interactions [145, 146]. Accordingly, in a full event simulation within such model there is no notion of an intermediate parton-level final state that is directly comparable to a resummed calculation. However, in SHERPA the parton showers off the hard process and the simulation of multiple-parton interactions are fully separated, *i.e.* the UE is simulated only after the shower evolution of the hard interaction is completed. The secondary scatterings then get showered and ultimately the partonic final state consisting of the showered hard process and multiple-parton interactions gets hadronized.

Accordingly, we here derive parton-to-hadron level transfer matrices for the jet angularities using the SHERPA generator. We obtain them from the same runs as the histograms shown as MC@NLO hadron-level SHERPA predictions in what follows. Besides the default hadronization tune we further determine a separate transfer matrix for each of the 7 replica tunes [111, 144] for the SHERPA cluster hadronization model [143]. We fold the resummed result, including each of the scale and x_L -parameter variations performed, with each of these matrices. The resulting envelope is then used as estimate for the total uncertainty of the prediction at hadron level.

When extracting the transfer matrices from SHERPA, we do allow for the possibility that non-perturbative corrections can reduce the transverse momentum of a given jet, and hence our cross section that is defined by requiring two jets of a certain hardness may become smaller. The sum of the probabilities for one parton-level bin to end up in any of the hadron-level bins is hence not guaranteed to be 1, and we indeed observe a significant loss of cross section when going from parton to hadron level. We however neglect the reverse effect, *i.e.* that a rather soft jet at parton level could pass the selection cut at hadron level, for example by picking up contributions from the underlying event. This is an important effect for example at the LHC, but appears not to be significant for our RHIC setup, consistent with the much reduced underlying event activity observed earlier.

To give an illustrative example we present in Fig. 5 the binned transfer matrices defined via Eq. (4.8) for the plain and **SoftDrop**-groomed LHA $\lambda_{1/2}$. In particular we here show the results corresponding to the nominal SHERPA hadronization tune and the event selections detailed in Sec. 2. In the 2D presentations the abscissa corresponds to the observable value at parton level, *i.e.* $\lambda_{1/2}^{\text{PL}}$, while the ordinate represents the observable at hadron level, *i.e.* $\lambda_{1/2}^{\text{HL}}$. Hence, a vertical line represents the binned probability for an event with given $\lambda_{1/2}^{\text{PL}} = v^{\text{PL}}$ to end up at some $\lambda_{1/2}^{\text{HL}}$ along the line. Similarly, a horizontal line at $\lambda_{1/2}^{\text{HL}} = v^{\text{HL}}$ indicates the likeliness for this hadron-level observation to originate from a given parton-level value $\lambda_{1/2}^{\text{PL}}$. Along with the transfer matrices, we here show the corresponding NLO + NLL' distribution at parton level (top of the panels) and hadron level (left-hand side of the panels), respectively. The latter are thereby obtained by convolving the former

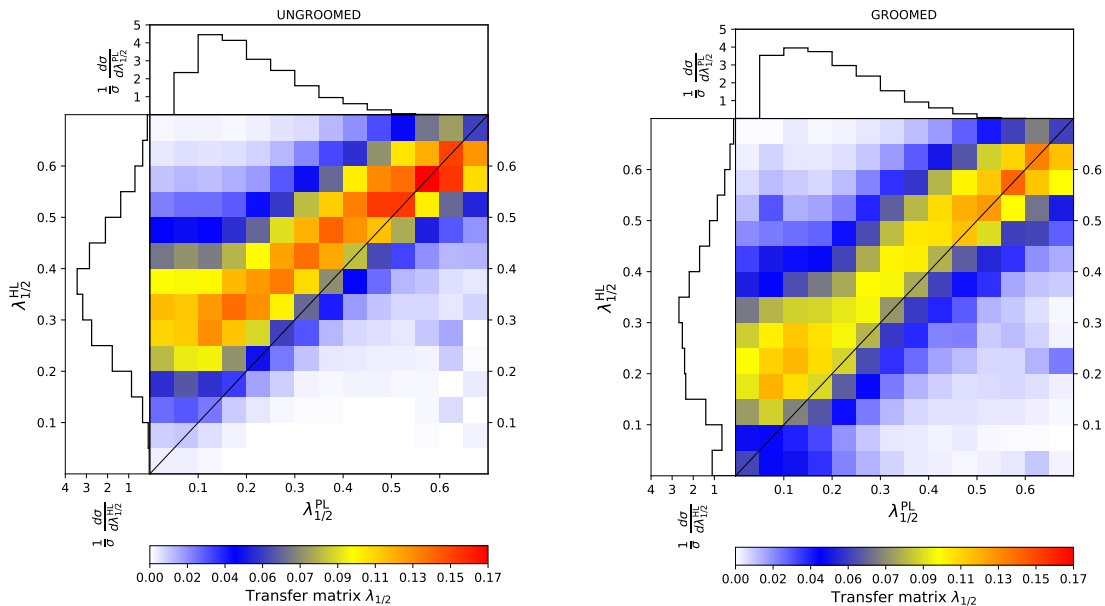


Figure 5: Transfer matrices defined according to Eq. (4.8) for the ungrooved (left) and groomed (right) angularity $\lambda_{1/2}$, extracted from SHERPA MC@NLO hadron-level simulations for the default hadronization tune.

with the given transfer matrix, resulting in our final NLO + NLL' + NP prediction.

For the ungrooved case we observe a significant shift of the parton-level observable towards higher values. In fact the transfer matrix has almost no entries in the lower triangle. Furthermore, the ridge of the 2D distribution appears rather broad and parallel shifted with respect to the diagonal. In particular for events with $\lambda_{1/2}^{\text{PL}} \lesssim 0.1$ the shift is even larger. Only for the tails of the distributions, *i.e.* $\lambda_{1/2} \geq 0.5$ is the transfer matrix largely diagonal and the hadron-level distribution receives non-negligible contributions also from higher parton-level values. For the groomed case, shown in the right panel, the hadronic corrections are on average somewhat reduced. There now appear a few entries also below the diagonal, corresponding to a reduction of the observable value from parton to hadron level. However, most of the time events still get shifted towards larger $\lambda_{1/2}^{\text{HL}}$, though the ridge of the 2D distribution now lies closer to the diagonal. As for the ungrooved case, beyond $\lambda_{1/2} \geq 0.5$ the transfer matrix is largely symmetric.

To capture the observed highly non-trivial migration in the angularity observables from parton to hadron level indeed requires the use of a somewhat sophisticated correction method, such as the transfer matrices employed here. In principle, observable-specific analytical corrections can be derived, modelling an additional non-perturbative emission, that is supposed to be soft [151]. The effect of such emission can be accounted for by an observable shift according to

$$\lambda_{\alpha}^{\text{HL}} = \lambda_{\alpha}^{\text{PL}} + \delta\lambda_{\alpha}^{\text{NP}}(\Omega), \quad (4.9)$$

where $\delta\lambda_{\alpha}^{\text{NP}}$ will depend on the observable value $\lambda_{\alpha}^{\text{PL}}$ and one or several non-perturbative

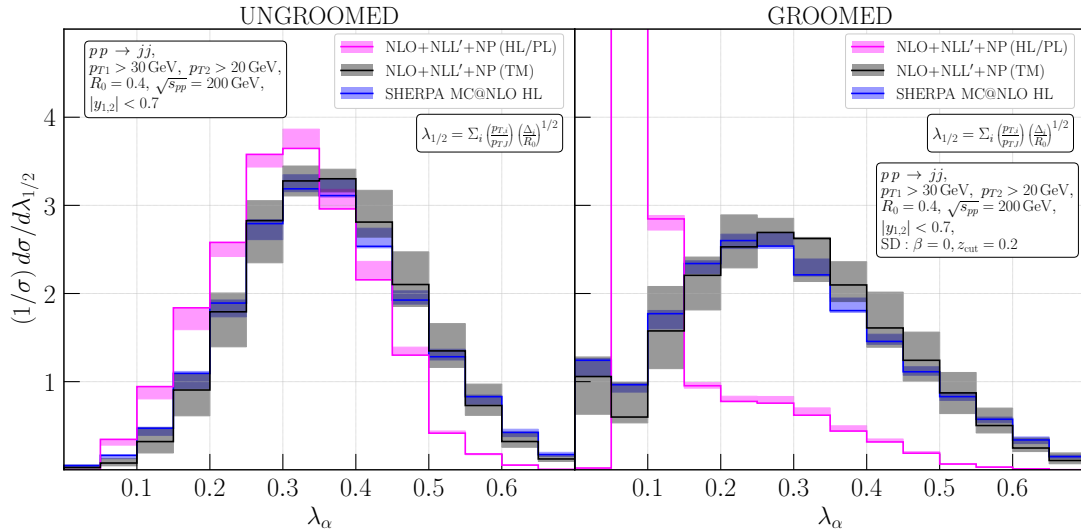


Figure 6: Hadron-level distributions for the $\lambda_{1/2}$ angularities without (left) and with **SoftDrop** grooming (right). Shown are hadron-level predictions from SHERPA along with two variants for correcting the NLO + NLL' parton-level result for non-perturbative corrections, through the transfer-matrix approach (grey) and the binwise multiplicative correction (purple).

parameters Ω , that need to be estimated. An application to **SoftDrop** thrust in electron-positron annihilation has been presented in Ref. [109].

Another alternative, based on Monte Carlo simulations at hadron and parton level, is a simple binwise multiplicative correction, according to

$$\lambda_{\alpha}^{\text{HL}} = \lambda_{\alpha}^{\text{PL}} \times \left(\frac{\lambda_{\alpha}^{\text{HL,MC}}}{\lambda_{\alpha}^{\text{PL,MC}}} \right). \quad (4.10)$$

To illustrate the latter method we present in Fig. 6 corresponding predictions for the above considered plain and groomed $\lambda_{1/2}^{\text{HL}}$ observables. Besides the hadron-level predictions from SHERPA and the NLO + NLL' + NP predictions obtained through the transfer-matrix approach, we show results for the multiplicative correction scheme. It is apparent that the binwise correction of the resummed distribution according to Eq. (4.10) yields significantly different results than the transfer-matrix method. The transfer-matrix corrections yield results very compatible with the SHERPA particle-level simulation. However, for the multiplicative correction, when considering the ungroomed case, the hadron-level result is significantly shifted towards lower angularity values. For the groomed case, in particular in the region below and around the parton-shower cutoff, *cf.* Fig. 2, the correction weights drastically overestimate the impact of non-perturbative effects. In consequence, for the normalized distribution the tail appears harshly suppressed. Accordingly, in what follows we will employ the transfer-matrix method to incorporate non-perturbative effects into our resummed predictions.

In Appendix A we provide an additional brief discussion regarding the relation of our transfer matrices and the shape-function approach of [152]. Therein, we also show illustrations of the transfer matrices for the groomed and ungroomed jet-width and jet-thrust angularities.

Hadron-level predictions for jet angularities in pp collisions

Having derived parton-to-hadron level transfer matrices specific for the six variants of jet angularities, *i.e.* $\lambda_{1/2}$, λ_1 and λ_2 with and without **SoftDrop** grooming, in dijet production in pp collisions at RHIC, with the fiducial phase space defined in Sec. 2, we can employ those to correct our NLO + NLL' predictions for non-perturbative effects.

In Fig. 7 we present our final hadron-level predictions referred to as NLO + NLL' + NP, based on the transfer matrices derived from SHERPA simulations. Alongside we show the corresponding particle-level predictions from SHERPA, based on parton-shower simulations at MC@NLO accuracy, supplemented with an UE simulation and hadronization. Such, these two predictions could in principle directly be compared to data from the sPHENIX experiment at RHIC when those are corrected for detector effects.

For both cases, we construct variants of the predictions from 7-point scale variations of the renormalization and factorization scale through on-the-fly reweighting [131], as well as from variations of hadronization-model parameters through 7 replica tunes [111, 144]. Note, for the SHERPA MC@NLO simulation, variations of the scales also affect the scales used in the initial- and final-state shower evolution. Within the resummed calculation however, we can vary the x_L parameter to obtain a more solid estimate of the logarithmic uncertainty. In both cases, the final uncertainty again is taken as the envelope of all variants, respectively.

For the normalized angularity distributions shown in Fig. 7 we observe excellent agreement between the two predictions. In fact, both results are fully compatible within their estimated uncertainties. In terms of the central values, the NLO + NLL' + NP calculation appears to predict a slightly softer, *i.e.* with a peak shifted to smaller angularity values, distribution for the Les Houches angularity $\lambda_{1/2}$. The distribution is also slightly wider, such that the tail towards the kinematic endpoint at large $\lambda_{1/2}$ is somewhat higher than in the SHERPA prediction. The general trend is reversed in the λ_1 case, where the Monte Carlo curve appears marginally shifted to smaller values. For λ_2 , the two distributions are very close and we can not make out any general trend. Again, any of these effects are covered by the uncertainties of the NLO + NLL' + NP calculation, and we conclude that at our accuracy there is no consistent systematic difference between the results. For the general physics features of the distributions we refer the reader back to our discussion in Sec. 3 and above in this part.

The estimated uncertainty of the SHERPA MC@NLO predictions is generally smaller than that of the matched resummed ones, consistent with the observations made in [77]. While the uncertainty estimate for the NLO + NLL' + NP prediction is somewhat larger, its size appears significantly reduced with respect to one for the partonic NLO + NLL' predictions shown in Fig. 1. At first sight this might seem counter intuitive, however, it can be traced back to the convolution with the parton-to-hadron level transfer matrices that largely smear out the sharp peaks at parton level.

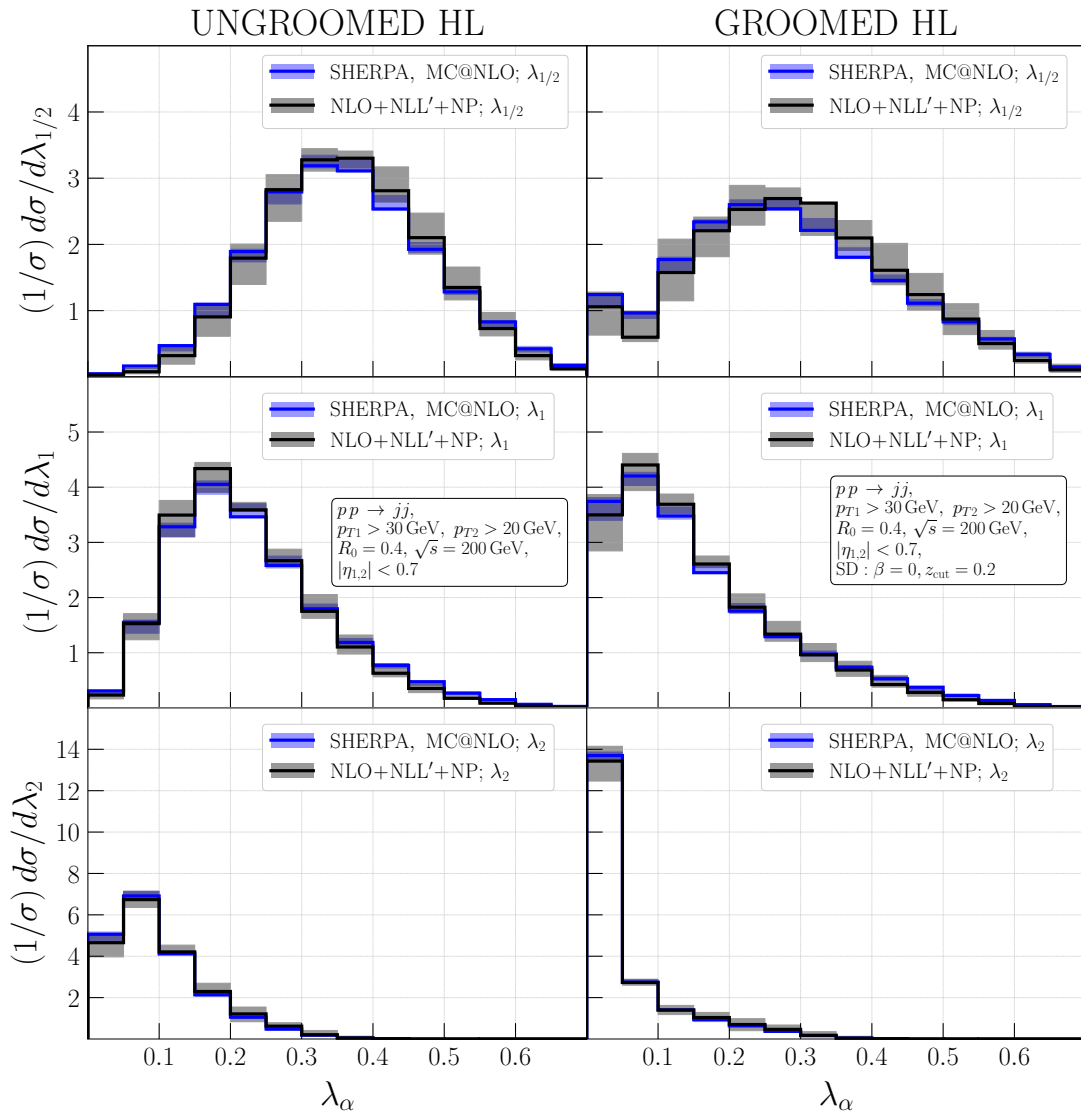


Figure 7: Hadron-level distributions for the $\lambda_{1/2}$, λ_1 , λ_2 angularities without (left) and with SoftDrop grooming (right). The shown NLO + NLL' predictions are corrected for non-perturbative effects using the transfer-matrix approach, dubbed NLO + NLL' +NP, and compared to corresponding particle-level simulations with SHERPA of MC@NLO accuracy.

Looking back at Fig. 5 it is apparent that the bulk of the hadron-level distribution, around $\lambda_{1/2}^{\text{HL}} \sim 0.3$, is largely made up of commensurate contributions from several bins of lower angularity at parton level, around $\lambda_{1/2}^{\text{PL}} \sim 0.1 - 0.25$. While in particular the x_L variations widely shift the peak of the parton-level distribution between these low angularity bins, this does not significantly alter their combined contribution to the bulk of the hadron-level result. Furthermore, the bins at very low λ^{PL} , featuring the largest uncertainties, are systematically pushed and broadly smeared out towards larger values of λ^{HL} .

Supported also by the good agreement of the SHERPA and PYTHIA results, presented

in Fig. 3, we are confident that the here presented NLO + NLL' +NP predictions provide reliable theoretical expectations for experimental measurements with sPHENIX at RHIC. Through a detailed comparison of jet-angularity observables in proton–proton collisions at RHIC energies the modelling of all-order perturbative corrections as well as non-perturbative aspects, in particular hadronization, can be thoroughly tested. For the here employed Monte Carlo simulations such data would furthermore provide useful means to tune and optimize model parameters associated with hadronization and the underlying event. Having established a good understanding of jet-substructure observables in pp collisions, these measurements can serve as a baseline for corresponding analyses in nucleus–nucleus scattering, thereby trying to infer about possible QCD-medium modifications.

5 Estimating medium-interaction effects on jet angularities

A high-density medium of deconfined quarks and gluons, referred to as Quark-Gluon Plasma (QGP) [153], can be formed in high-energy heavy-ion collisions. The characteristic scale of a QGP is expected to be an order of magnitude larger than the QCD confinement scale, $\Lambda_{\text{QCD}} \approx 0.2 \text{ GeV}$. Hard QCD processes initiating the production of particles with sufficiently high transverse momenta, such that the hierarchy $p_{T,\text{jet}} \gg \Lambda_{\text{QGP}} \gg \Lambda_{\text{QCD}}$ holds, can be considered as factorized from later interactions with the QGP medium [154]. However, the multiple soft and collinear subsequent emissions leading to jet formation are expected to be affected by medium-induced interactions giving rise to a broad range of jet-quenching phenomena [155–161]. Qualitatively, jet quenching embraces three distinct effects: Energy loss, *i.e.* the reduction of the energy of particles inside a jet or the jet energy as a whole [155], leading to the suppression of cross sections; an increase in the number of soft particles inside the jet, *i.e.* the softening of jet fragmentation [156, 158]; and jet broadening, *i.e.* an increase in the number of soft particles displaced away from the jet axis [162–167].

In fact, all these jet-quenching effects are expected to affect the jet angularities as defined in Eq. (2.2). Various dedicated MC programs were developed that aim to simulate jet-quenching effects, including HIJING [157], JEWEL [93], PQM [168], HYBRID [169] and Q-PYTHIA [92]. Apart from these codes there exists the general JETSCAPE framework [170] capable of simulating jet propagation through a QGP medium based on the usage of various hydrodynamical models [171–175]. In this paper we would like to provide a qualitative estimate of quenching effects for jet angularities in AA collisions at RHIC energies, *i.e.* $\sqrt{s_{\text{NN}}} = 200 \text{ GeV}$. Given hydrodynamical simulations can easily be very time-consuming, we reserve using the JETSCAPE framework for future work and consider only two rather light-weighted MC choices, namely Q-PYTHIA and JEWEL, both based upon modified versions of the PYTHIA 6 virtuality-ordered parton shower [71].

Medium-effect simulations based on Q-PYTHIA and JEWEL

The Q-PYTHIA model is based upon the addition of an extra term to the standard Altarelli–Parisi shower splitting kernels $P_{\text{vac}}(z)$ [176], according to

$$P_{\text{tot}}(z) = P_{\text{vac}}(z) + \Delta P(z, t, \hat{q}, L, E), \quad (5.1)$$

where $\Delta P(z, t, \hat{q}, L, E)$ accounts for medium modifications in dependence on the virtuality t of the radiating parton, its energy E , the medium length L , and the transport coefficient \hat{q} . Whereas vacuum splitting functions $P_{\text{vac}}(z)$ are well known and can be derived from first-principles perturbative QCD calculations, the additional term in Eq. (5.1) is a priori unknown and in general cannot be evaluated by means of perturbation theory only. However, the medium-induced splitting functions can be obtained within the Baier–Dokshitzer–Mueller–Peigné–Schiff–Zakharov (BDMPS-Z) formalism [177–183], where interactions between QCD parton-shower particles and the QGP medium get approximated by an infinite number of soft scatterings². The residual dependence on non-perturbative physics is encoded in the time-dependent density of scattering centers $n(\xi)$ and the single dipole elastic scattering cross section $\sigma(\mathbf{r})$ which are related to the time-dependent transport coefficient \hat{q} via

$$n(\xi)\sigma(\mathbf{r}) = \frac{1}{2}\hat{q}(\xi)\mathbf{r}^2, \quad (5.2)$$

where $\hat{q}(\xi)$ is interpreted as the medium induced transverse momentum squared $\langle q_{\perp}^2 \rangle_{\text{med}}$ per unit path length λ [161, 178, 188]. As a further simplification Q-PYTHIA assumes \hat{q} to be time-independent which corresponds to a static uniform QGP medium. As a consequence, the transport coefficient \hat{q} becomes the only free non-perturbative parameter within the Q-PYTHIA model. In what follows we will assume its value to be given by

$$\hat{q} = 2 \text{ GeV}^2/\text{fm}. \quad (5.3)$$

More information on the way Q-PYTHIA evaluates the splitting kernels in Eq. (5.1) can be found in Refs. [164, 177, 184, 190].

Another MC generator to account for QGP medium effects is JEWEL (Jet Evolution With Energy Loss) [93, 191, 192]. Similar to Q-PYTHIA, the approach of JEWEL is based upon modification of the PYTHIA 6 parton-shower model by including $2 \rightarrow 2$ rescatterings between shower partons and additional “external” partons representing QGP scattering centers. These rescatterings change the virtuality of the shower partons which afterwards may continue to participate in the parton-shower evolution [93, 191, 193, 194]. Apart from that, JEWEL also contains a Monte Carlo model for the suppression of gluon spectra at energy scales smaller than $w_c = \hat{q}L^2/2$ caused by destructive interference in elastic scattering between emitted gluons and the QGP medium also known as non-abelian analog of the Landau–Pomeranchuk–Migdal (LPM) [159, 195–197] effect. The JEWEL approach to model medium effects is fully microscopic and the only required assumption on QGP properties is the density of scattering centers which can be evaluated using different models. The default medium model of JEWEL [191, 198] is based upon the Bjorken model of an ideal quark–gluon gas [199] and some Glauber calculations [200]. For definiteness, in what follows we assume for the medium temperature a value of $T = 0.55 \text{ fm}$. Furthermore, the overlap between colliding nuclei in the Glauber calculations is limited to the centrality class $[0, 10]\%$.

Finally, we would like to note that the overall particle multiplicity in AA collisions is typically about hundred times larger than in pp collisions. Such drastic increase is due to the

²For phenomenological applications of the BDMPS-Z approach see Refs. [160, 184–189].

production of additional soft particles via multiple nucleon–nucleon interactions and, presumably, the hadronization of the QGP medium. Therefore, the presence of such additional soft background in AA collisions may require the application of event-wide background removal techniques other than `SoftDrop` grooming we were using in the previous sections. This issue will be addressed below.

Hadron-level predictions for jet angularities in AA collisions at RHIC

We present our results for the three angularities λ_α where $\alpha \in \{1/2, 1, 2\}$ without and including the subtraction of soft-background particles in Figs. 8 and 9, respectively. Fig. 8 contains vacuum-level predictions from Q-PYTHIA (blue solid line) and JEWEL (red solid line), corresponding to the expectations for pp collisions. For comparison, we also include our NLO+NLL' predictions corrected for non-perturbative effects as presented in Section 4. These results get contrasted with Q-PYTHIA (blue dashed line) and JEWEL (red dashed line) simulations taking into account medium effects. The medium Q-PYTHIA result does not contain particles from the bulk, soft background, whereas the medium JEWEL result by default contains such soft particles. These soft background particles can easily wash out the parton-shower emission pattern. In Fig. 8 we do not consider any soft-background removal measures which can be physically implemented in experiments. Instead, in order to evaluate the intrinsic modification of jets without the background contamination, we provide the medium JEWEL result without the “recoil particles” (red dashed line) by using an internal particle tag for medium particles in the JEWEL simulation. In reality, such recoil particles are included in jet reconstruction and can not be physically separated from the jet. Therefore this “NO REC” JEWEL result should only represent an “ideally” background subtracted result and is meant to show qualitative features of JEWEL medium effects. For the `SoftDrop` groomer we employed the same parameters as in Sections 3 and 4.

We observe that the vacuum-level predictions obtained with JEWEL and Q-PYTHIA wrap the NLO + NLL' + NP results, with JEWEL predicting somewhat broader, Q-PYTHIA somewhat narrower spectra. While the agreement among these two LO simulations is certainly not perfect, differences are mild when considering that no efforts were made to enforce a tuned comparison, but rather the default settings of both generators have been employed here. Although both codes are based upon modified versions of PYTHIA 6, their setups for pp vacuum simulations are not identical. For example, Q-PYTHIA employs the ATLAS MC09 tune [201], the CTEQ 5L LO PDFs [202], and is based on PYTHIA 6.4.18. JEWEL, in contrast, uses the CT14 NLO PDFs [203] and is derived from PYTHIA 6.4.25. While a more detailed analysis of the origin of the deviations between the two generator predictions is interesting, this is considered beyond the scope of the present paper. We envisage a dedicated measurement of the considered jet angularities in pp collisions at sPHENIX that could then eventually be used to align parameter choices in the simulations to obtain a satisfactory description of the pp-baseline results.

The AA simulation results shown in Fig. 8 demonstrate significant differences compared to the vacuum-level predictions just discussed. We find that both Q-PYTHIA and JEWEL with QGP medium effects being turned on predict jet-angularity distributions significantly different from the “reference” vacuum-level results, especially for the Q-PYTHIA

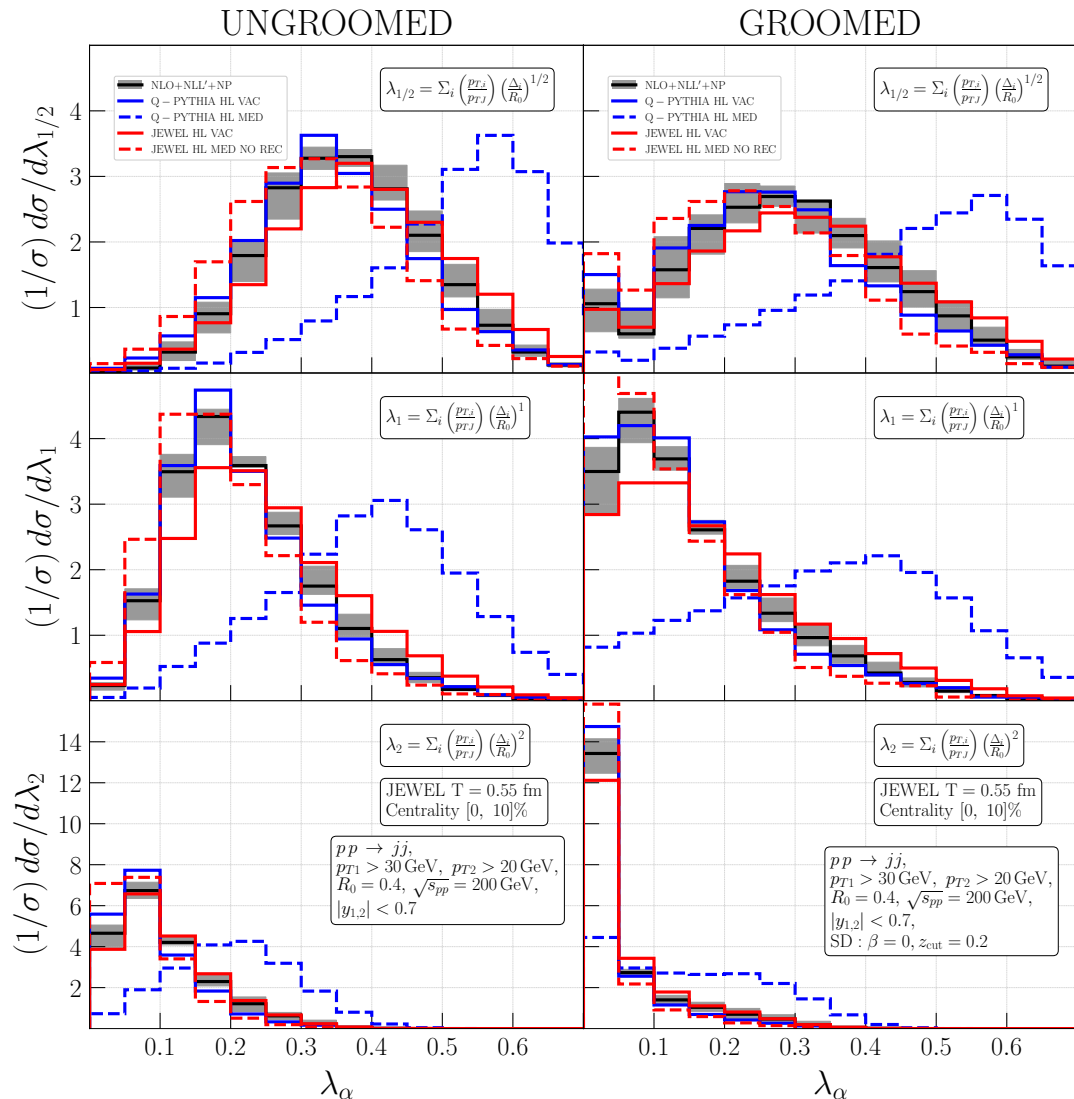


Figure 8: Q-PYTHIA and JEWEL predictions for jet-angularity distributions in pp (solid lines) and AA (dashed lines) collisions at RHIC, without physical soft-background subtraction. Furthermore, the hadron-level corrected resummed predictions of NLO + NLL' accuracy are shown in black.

result. It is apparent that JEWEL and Q-PYTHIA, while providing similar results for the vacuum case, produce quite different medium-level distributions which significantly deviate from each other, corresponding to their different methods to account for medium effects in AA collisions. The Q-PYTHIA ansatz of modifying the QCD splitting functions preserves parton-shower unitarity and, as a consequence, the total energy of all final-state particles produced in a given event always equals the initial nucleon–nucleon center-of-mass energy. Accordingly, any increase in soft-particle production is compensated for by a decrease of the momentum of the leading partons inside a jet caused by the energy–momentum con-

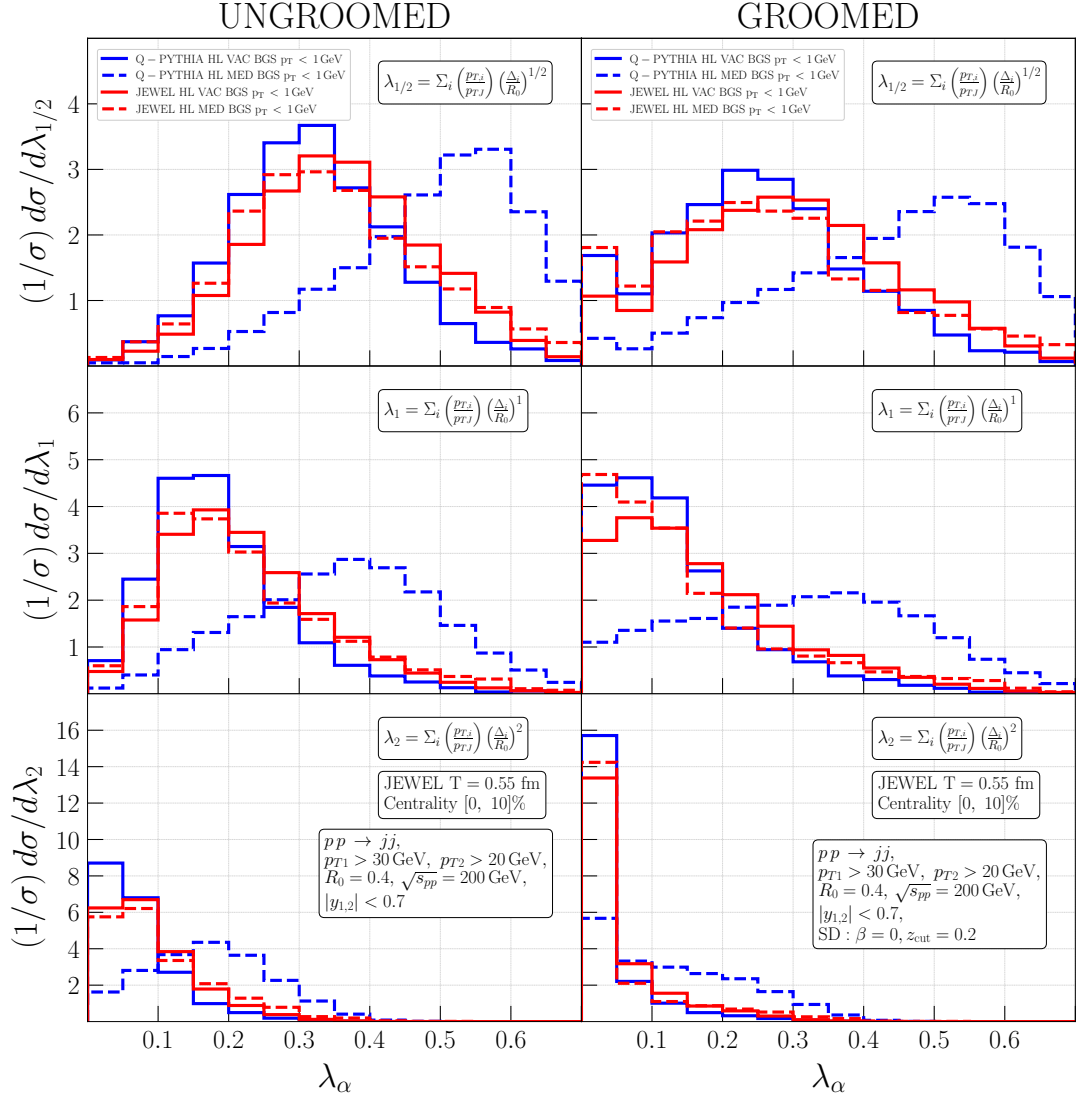


Figure 9: Q-PYTHIA and JEWEL predictions for jet-angularity distributions in pp (solid lines) and AA (dashed lines) collisions at RHIC, with soft-background subtraction, *i.e.* after removal of soft particles with $p_T < 1$ GeV from the final state.

servation constraint. For JEWEL, the medium effect comes from jet particles scattering with medium particles with momentum transfer. These medium particles can be traced as recoil particles after collisions. Qualitatively, in the Q-PYTHIA model the medium greatly increases the values of jet angularities even for **SoftDrop** groomed jets. This may imply that the modified splitting functions can significantly affect hard branching kinematics. In contrast, the JEWEL result shows that the medium decreases the values of jet angularities, which may be caused by loss of energy and particles inside the jet.

There are various sophisticated background-removal techniques described in the literature on heavy-ion physics [39, 204, 205]. However, in this rather qualitative study we

decided to consider just a simple subtraction of final-state particles with $p_T < 1$ GeV. While one might expect that **SoftDrop** grooming helps to clean up jets from the thermal background, this technique was specifically constructed to subtract soft wide-angle radiation with respects to the jet axis. Soft particles included in the hard branching that satisfy the **SoftDrop** condition therefore remain in the jet. In Fig. 9 we present our corresponding Q-PYTHIA and JEWEL default (therefore including the soft recoil particles in the simulation output) results for the jet angularities, with soft particles removed from the final state prior to jet clustering and the application of the event-selection criteria. Note, such procedure effectively defines new observables which do not obey the concept of infrared and collinear (IRC) safety which forms a corner stone of the here employed CAESAR resummation technique. Accordingly, we here do not include our NLO+NLL'+NP predictions, given it is not completely clear how to consistently correct them for such soft-background subtraction³.

By comparing the results shown in Figs. 8 and 9 we observe that the removal of soft particles with $p_T < 1$ GeV mildly affects the Q-PYTHIA results, both for the vacuum simulations as well as for the AA runs. However, it effectively removes soft recoil particles in the JEWEL medium-level simulations, producing a distribution (dashed red line in Fig. 9) which is close to the medium-level distribution without recoil particles (dashed red line in Fig. 8) and also the vacuum-level distribution (solid red line in Fig. 9). The stability of the Q-PYTHIA results with respect to the removal of soft particles below 1 GeV can be explained by the fact that the Q-PYTHIA model is based on the modification of the QCD emission pattern according to Eq. (5.1), thereby, essentially, imposing a redistribution of energy between soft and hard particles produced inside a given jet due to the interaction with the external QGP medium. Accordingly, soft final-state particles produced in AA simulations with Q-PYTHIA cannot directly be interpreted as a thermal QCD background from overlaid nucleon–nucleon interactions that produce uniformly distributed soft particles with very low energies. In Fig. 10 we further show the Q-PYTHIA results with a more stringent cut to remove soft particles below 2 GeV, and the medium modification pattern remains significant.

Finally, we would like to note that the JEWEL AA simulations after removal of soft particles with $p_T < 1$ GeV, which may include both jet and medium particles, differ marginally with the corresponding pp results. The differences between the vacuum-level Q-PYTHIA and JEWEL results is sometimes even larger than the difference between vacuum-level and medium-level distributions from JEWEL. That is, the uncertainty of vacuum-level Monte Carlo predictions is larger than the size of the medium effect JEWEL predicts. We therefore conclude that a detailed comparison of vacuum-level simulations against experimental data collected at RHIC in pp collisions will be of utmost importance to validate and challenge the available theoretical predictions based on the intriguing combination of perturbative

³We remark that a possible approach to partially account for soft-background subtraction could proceed through the extraction of corresponding transfer-matrices, where at hadron-level the particle- p_T threshold criterion is invoked, see for example Ref. [110] for a related discussion of charged-track based hadronic event-shape distributions. However, such procedure would effectively assume that all soft particles with momentum below the particle- p_T threshold are described by non-perturbative QCD and hence can be considered separately from the resummed calculations. An assumption that remains to be verified.

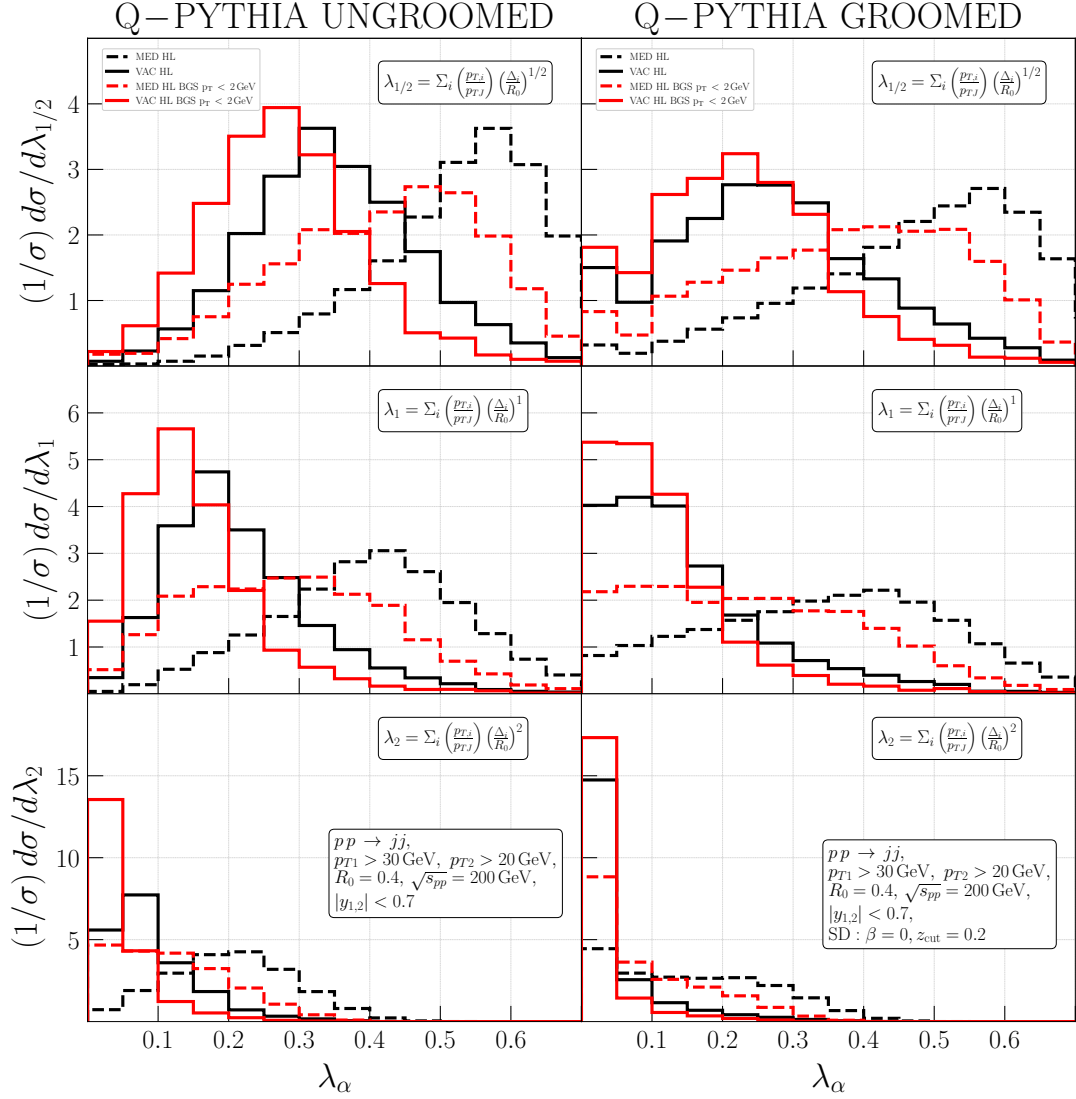


Figure 10: Q-PYTHIA predictions for jet-angularity distributions in pp (solid lines) and AA (dashed lines) collisions at RHIC, with (red lines) and without (black lines) soft-background subtraction, *i.e.* after removal of soft particles with $p_T < 2$ GeV from the final state.

and non-perturbative QCD phenomena. Besides Monte Carlo simulation tools this also includes analytic predictions based on all-order resummation, corrected for hadronization and underlying event effects. Such detailed comparison will allow us to establish a baseline for the understanding of jet substructure in pp collisions at RHIC which is necessary for getting control over jet-substructure studies in AA scattering events.

6 Conclusions

Jet-substructure measurements provide unique insights into the dynamics of QCD and constitute a superb testbed for theoretical approaches. In this study we considered the

well-known class of jet-angularity observables for the case of pp and AA collisions at RHIC. Thereby the pp setup serves as a rather well understood and well controlled reference towards studying the impact of medium-effects as anticipated from the creation of a QGP in heavy-ion collisions.

To this end, we derived NLO + NLL' accurate predictions for three distinct angularities of QCD jets, with and without `SoftDrop` grooming, produced in pp collisions corresponding to the setup of the sPHENIX experiment currently operating at RHIC. To account for non-perturbative effects from underlying event and hadronization, we correct our predictions with the help of transfer matrices which have been shown to provide a better description of collider data than a simple multiplicative reweighting approach [77]. Our detailed study of non-perturbative contributions demonstrated a dominant rôle of hadronization corrections and a suppression of contributions from multi-parton interactions compared to an earlier LHC study [77]. Accordingly, we claim that dedicated jet-substructure studies in pp collisions at RHIC can, to a large extent, help to disentangle and constrain hadronization effects from the underlying event which is clearly not possible at the LHC due to the much higher beam energy.

The NLO + NLL' resummed predictions corrected for non-perturbative results were compared against SHERPA simulations of MC@NLO accuracy and indeed very good agreement between the two results, taking into account theoretical uncertainties, was found. We envisage that a future measurement of sPHENIX and the detailed comparison against our and other theoretical predictions will help to further probe and constrain MC models for non-perturbative effects in pp collisions at energies much lower than at LHC.

While we consider the NLO + NLL' + NP and MC@NLO SHERPA predictions a main deliverable of this paper, we also provided a qualitative estimate for the impact of QGP medium-effects on jet-substructure observables. To this end, we simulated AA collisions with two MC generators, namely Q-PYTHIA and JEWEL. We found that the jet-angularity predictions from Q-PYTHIA and JEWEL show a significantly different behavior. Whereas the default JEWEL setting simulates high-multiplicity soft-particle production originating from the external QGP media, Q-PYTHIA modifies the parton-shower splitting kernels according to the BDMPS-Z formalism, resulting in an increased emission of soft particles from the hard-process final state. Accordingly, their multiplicity is limited by energy-momentum conservation, *i.e.* the constraint that the energies of all final-state particles have to sum up to the nucleon-nucleon center-of-mass energy. This, as was also argued in the original Q-PYTHIA publication [92], can be seen as a limitation of the current model since in AA collisions multiple soft particles can furthermore be produced due to the thermalization of the QGP and additional nucleon-nucleon interactions, such that the total energy of all final-state particles can easily exceed $\sqrt{s_{\text{NN}}}$. Q-PYTHIA predicts a significant enhancement of jet angularity values. On the other hand, by comparing the JEWEL jet angularity predictions for pp and AA (without recoil particles) collisions, a significant decrease of jet angularity values was observed in JEWEL. After soft-background subtraction, the jet angularity predictions for AA collisions simulated with JEWEL showed very moderate medium modifications compared to the vacuum-level results, whereas the Q-PYTHIA AA results still exhibit striking differences. Given that jet-substructure modifications observed in previous

experiments do not tend to support such strong effects compared to pp results [68], we would assume that after detailed comparison against upcoming new results from sPHENIX the Q-PYTHIA model may need to be revised. We also argue that the observed marginal difference between JEWEL pp and AA results after background removal, as compared to the difference between JEWEL and Q-PYTHIA pp predictions, highlights the importance of precision understanding of the pp results in order to meaningfully extract medium modifications. Whereas in this paper we used a simple removal of final-state particles with $p_T < 1$ GeV, a more sophisticated background-subtraction technique such as described in Refs. [39, 204, 205] should be used when comparing Monte Carlo predictions against data. Each of these techniques, in turn, leads to somewhat differently defined jet-substructure observables and hence requires a dedicated investigation and analytic understanding which we leave to future studies.

Acknowledgments

SS acknowledges support from BMBF (05H21MG CAB) and from Deutsche Forschungsgemeinschaft (DFG, German Research Foundation) — project number 456104544. The work of DR was supported by the STFC IPPP grant (ST/T001011/1). The work of OF and YTC is supported in part by the US Department of Energy (DOE) Contract No. DE-AC05-06OR23177, under which Jefferson Science Associates, LLC operates Jefferson Lab, and by the Department of Energy Early Career Award grant DE-SC0023304. We are grateful to Liliana Apolinário and Néstor Armesto for providing the version of the Q-Pythia code specifically tuned for the RHIC setup. We also would like to thank Roli Esha and Megan Connors for useful and fruitful discussions on the potential of the sPHENIX experiment for jet angularity measurements. Most of the simulation is conducted with computing facilities of the Galileo cluster at the Department of Physics and Astronomy of Georgia State University.

A Connection between transfer matrices and shape functions

The non-perturbative power corrections of general infrared and collinear (IRC) safe jet-substructure observables may be included by convolving the resummed, perturbative calculations with the corresponding shape functions originally introduced by Korchemsky and Sterman [152]. For jet angularities, the convolution may take the following form [85, 206] if the non-perturbative correction is naively modeled by a single-scale contribution⁴,

$$\frac{d\sigma}{d\lambda_\alpha^{\text{HL}}} = \int d\epsilon f(\epsilon) \int d\lambda_\alpha^{\text{PL}} \frac{d\sigma}{d\lambda_\alpha^{\text{PL}}} \delta\left(\lambda_\alpha^{\text{HL}} - \lambda_\alpha^{\text{PL}} - C_\alpha^{\beta, z_{\text{cut}}} \epsilon^{\gamma_\alpha^\beta}\right), \quad (\text{A.1})$$

where the function $f(\epsilon)$ is the shape function of the jet angularity λ_α . Its functional argument ϵ is the low energy contribution to λ_α from the non-perturbative soft momenta. Here we suppress the dependence of the observable on the soft-drop parameters β and z_{cut}

⁴The non-perturbative corrections to `SoftDrop` jet mass was studied in details in [148, 207]. There the shape function is involved in a non-trivial convolution caused by the `SoftDrop` procedure.

for simplicity. Because of the additivity of jet angularities from individual jet-constituent momenta, the value of the observable at hadron level ($\lambda_\alpha^{\text{HL}}$) is offset from the value at parton level ($\lambda_\alpha^{\text{PL}}$) by an amount $C_\alpha^{\beta, z_{\text{cut}}} \epsilon \gamma_\alpha^\beta$. The coefficient $C_\alpha^{\beta, z_{\text{cut}}}$ and the power γ_α^β in general depend on the angularity and soft-drop parameters. Here we can use a power-counting argument to derive the dependence on these parameters. The measurement of λ_α constrains the values of z and Δ of a particle emission,

$$\lambda_\alpha \sim z \left(\frac{\Delta}{R_0} \right)^\alpha. \quad (\text{A.2})$$

On the other hand, the **SoftDrop** procedure induces another constraint through the **SoftDrop** condition,

$$z \sim z_{\text{cut}} \left(\frac{\Delta}{R_0} \right)^\beta. \quad (\text{A.3})$$

These two constraints then determine the values of z and Δ ,

$$z \sim z_{\text{cut}} \left(\frac{\lambda_\alpha}{z_{\text{cut}}} \right)^{\frac{\beta}{\alpha+\beta}}, \quad \Delta \sim R_0 \left(\frac{\lambda_\alpha}{z_{\text{cut}}} \right)^{\frac{1}{\alpha+\beta}}, \quad (\text{A.4})$$

which induces the following characteristic energy scale ϵ ,

$$\epsilon \sim p_T z \Delta \sim p_T z_{\text{cut}} R_0 \left(\frac{\lambda_\alpha}{z_{\text{cut}}} \right)^{\frac{1+\beta}{\alpha+\beta}}. \quad (\text{A.5})$$

Non-perturbative soft physics at this scale may contribute to the angularity value by an amount $\delta\lambda_\alpha$, where

$$\delta\lambda_\alpha \sim z_{\text{cut}} \left(\frac{\epsilon}{p_T z_{\text{cut}} R_0} \right)^{\frac{\alpha+\beta}{1+\beta}}. \quad (\text{A.6})$$

In this case $C_\alpha^{\beta, z_{\text{cut}}} \sim z_{\text{cut}} \left(1/p_T z_{\text{cut}} R_0 \right)^{\frac{\alpha+\beta}{1+\beta}}$ and $\gamma_\alpha^\beta \sim \frac{\alpha+\beta}{1+\beta}$.

After integrating out the soft momentum variable ϵ , the hadronic cross section can be expressed in the following integral form,

$$\frac{d\sigma}{d\lambda_\alpha^{\text{HL}}} = \int d\lambda_\alpha^{\text{PL}} \frac{d\sigma}{d\lambda_\alpha^{\text{PL}}} \left[\frac{1}{C_\alpha^{\beta, z_{\text{cut}}} \gamma_\alpha^\beta} \left(\frac{\lambda_\alpha^{\text{HL}} - \lambda_\alpha^{\text{PL}}}{C_\alpha^{\beta, z_{\text{cut}}}} \right)^{\frac{1}{\gamma_\alpha^\beta} - 1} f \left(\left(\frac{\lambda_\alpha^{\text{HL}} - \lambda_\alpha^{\text{PL}}}{C_\alpha^{\beta, z_{\text{cut}}}} \right)^{\frac{1}{\gamma_\alpha^\beta}} \right) \right] \quad (\text{A.7})$$

$$= \int d\lambda_\alpha^{\text{PL}} \frac{d\sigma}{d\lambda_\alpha^{\text{PL}}} \mathcal{T}(\lambda_\alpha^{\text{HL}} | \lambda_\alpha^{\text{PL}}), \quad (\text{A.8})$$

where the term in the square brackets can be identified as the transfer matrix $\mathcal{T}(\lambda_\alpha^{\text{HL}} | \lambda_\alpha^{\text{PL}})$ interpreted as the conditional probability of $\lambda_\alpha^{\text{HL}}$, given the value of $\lambda_\alpha^{\text{PL}}$ before the non-perturbative process. The naive convolution of the shape function implies that the transfer matrix depends only on $\lambda_\alpha^{\text{HL}} - \lambda_\alpha^{\text{PL}}$. The extracted transfer matrices in our work roughly show a consistent trend with equal probability along the diagonal lines of constant $\lambda_\alpha^{\text{HL}} - \lambda_\alpha^{\text{PL}}$ in a restricted region of angularity, see Fig. 5 in Section 4 and Figs. 11 and 12 provided in this appendix. By projecting the transfer matrix onto a constant $\lambda_\alpha^{\text{HL}} + \lambda_\alpha^{\text{PL}}$ line we may extract the shape function consistent with the Monte Carlo non-perturbative correction. In fact, the extracted transfer matrix does not follow the scaling of $\lambda_\alpha^{\text{HL}} - \lambda_\alpha^{\text{PL}}$ especially in the large or small angularity regions. Therefore the transfer matrix can be a general approach to quantify non-perturbative corrections.

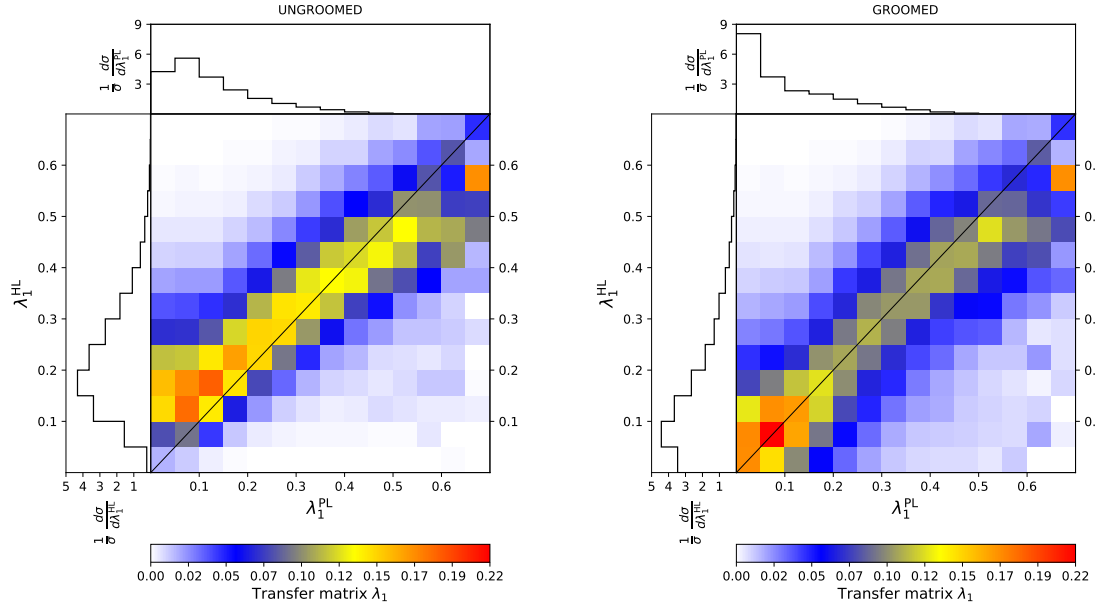


Figure 11: Transfer matrices defined according to Eq. (4.8) for the ungroomed (left) and groomed (right) angularity λ_1 , extracted from SHERPA MC@NLO hadron-level simulations for the default hadronisation tune.

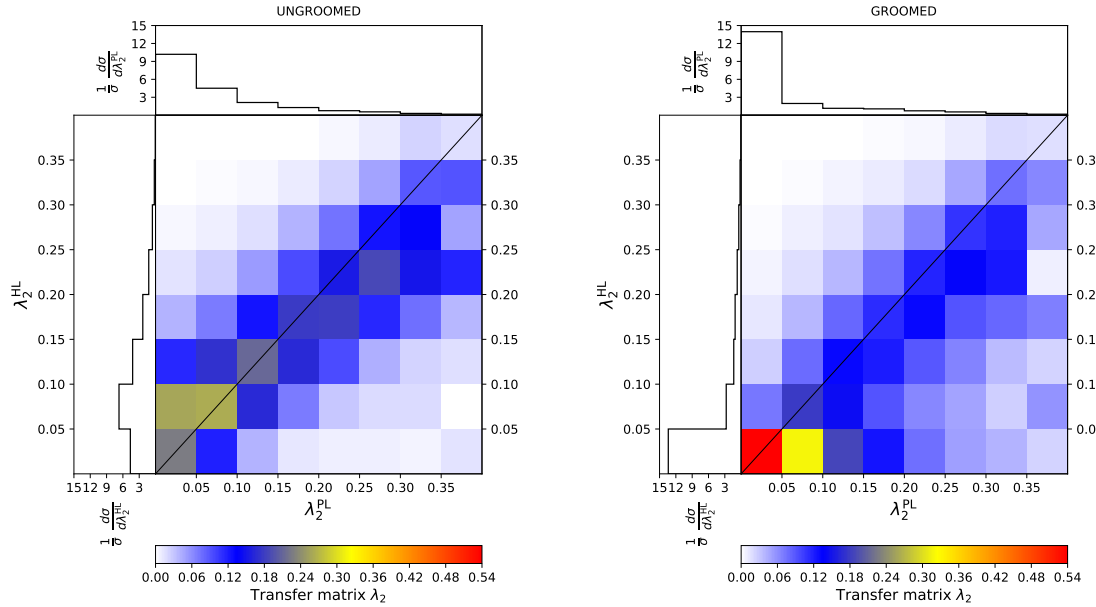


Figure 12: Transfer matrices defined according to Eq. (4.8) for the ungroomed (left) and groomed (right) angularity λ_2 , extracted from SHERPA MC@NLO hadron-level simulations for the default hadronisation tune.

References

- [1] D. Britzger, K. Rabbertz, D. Savoiu, G. Sieber, and M. Wobisch, *Determination of the strong coupling constant using inclusive jet cross section data from multiple experiments*, *Eur. Phys. J. C* **79** (2019), no. 1 68, [[arXiv:1712.00480](#)].
- [2] **CMS** Collaboration, S. Chatrchyan et al., *Measurement of the Ratio of the Inclusive 3-Jet Cross Section to the Inclusive 2-Jet Cross Section in pp Collisions at $\sqrt{s} = 7$ TeV and First Determination of the Strong Coupling Constant in the TeV Range*, *Eur. Phys. J. C* **73** (2013), no. 10 2604, [[arXiv:1304.7498](#)].
- [3] **ATLAS** Collaboration, M. Aaboud et al., *Determination of the strong coupling constant α_s from transverse energy–energy correlations in multijet events at $\sqrt{s} = 8$ TeV using the ATLAS detector*, *Eur. Phys. J. C* **77** (2017), no. 12 872, [[arXiv:1707.02562](#)].
- [4] **ATLAS** Collaboration, G. Aad et al., *Measurement of transverse energy-energy correlations in multi-jet events in pp collisions at $\sqrt{s} = 7$ TeV using the ATLAS detector and determination of the strong coupling constant $\alpha_s(m_Z)$* , *Phys. Lett. B* **750** (2015) 427–447, [[arXiv:1508.01579](#)].
- [5] **CMS** Collaboration, V. Khachatryan et al., *Measurement of the inclusive 3-jet production differential cross section in proton–proton collisions at 7 TeV and determination of the strong coupling constant in the TeV range*, *Eur. Phys. J. C* **75** (2015), no. 5 186, [[arXiv:1412.1633](#)].
- [6] **ATLAS** Collaboration, G. Aad et al., *Determination of the parton distribution functions of the proton from ATLAS measurements of differential W and Z boson production in association with jets*, *JHEP* **07** (2021) 223, [[arXiv:2101.05095](#)].
- [7] **ATLAS** Collaboration, G. Aad et al., *Measurement of the inclusive jet cross section in pp collisions at $\sqrt{s}=2.76$ TeV and comparison to the inclusive jet cross section at $\sqrt{s}=7$ TeV using the ATLAS detector*, *Eur. Phys. J. C* **73** (2013), no. 8 2509, [[arXiv:1304.4739](#)].
- [8] **CMS** Collaboration, V. Khachatryan et al., *Constraints on parton distribution functions and extraction of the strong coupling constant from the inclusive jet cross section in pp collisions at $\sqrt{s} = 7$ TeV*, *Eur. Phys. J. C* **75** (2015), no. 6 288, [[arXiv:1410.6765](#)].
- [9] **CMS** Collaboration, V. Khachatryan et al., *Measurement and QCD analysis of double-differential inclusive jet cross sections in pp collisions at $\sqrt{s} = 8$ TeV and cross section ratios to 2.76 and 7 TeV*, *JHEP* **03** (2017) 156, [[arXiv:1609.05331](#)].
- [10] R. Abdul Khalek et al., *Phenomenology of NNLO jet production at the LHC and its impact on parton distributions*, *Eur. Phys. J. C* **80** (2020), no. 8 797, [[arXiv:2005.11327](#)].
- [11] L. A. Harland-Lang, A. D. Martin, and R. S. Thorne, *The Impact of LHC Jet Data on the MMHT PDF Fit at NNLO*, *Eur. Phys. J. C* **78** (2018), no. 3 248, [[arXiv:1711.05757](#)].
- [12] J. Pumplin, J. Huston, H. L. Lai, P. M. Nadolsky, W.-K. Tung, and C. P. Yuan, *Collider Inclusive Jet Data and the Gluon Distribution*, *Phys. Rev. D* **80** (2009) 014019, [[arXiv:0904.2424](#)].
- [13] B. J. A. Watt, P. Motylinski, and R. S. Thorne, *The Effect of LHC Jet Data on MSTW PDFs*, *Eur. Phys. J. C* **74** (2014) 2934, [[arXiv:1311.5703](#)].
- [14] **CMS** Collaboration, A. Tumasyan et al., *Study of quark and gluon jet substructure in Z+jet and dijet events from pp collisions*, *JHEP* **01** (2022) 188, [[arXiv:2109.03340](#)].

- [15] **ALICE** Collaboration, S. Acharya et al., *Measurements of the groomed and ungroomed jet angularities in pp collisions at $\sqrt{s} = 5.02$ TeV*, *JHEP* **05** (2022) 061, [[arXiv:2107.11303](#)].
- [16] D. E. Soper and M. Spannowsky, *Combining subjet algorithms to enhance ZH detection at the LHC*, *JHEP* **08** (2010) 029, [[arXiv:1005.0417](#)].
- [17] R. M. Godbole, D. J. Miller, K. A. Mohan, and C. D. White, *Jet substructure and probes of CP violation in Vh production*, *JHEP* **04** (2015) 103, [[arXiv:1409.5449](#)].
- [18] N. Chen, J. Li, Y. Liu, and Z. Liu, *LHC searches for the CP-odd Higgs by the jet substructure analysis*, *Phys. Rev. D* **91** (2015), no. 7 075002, [[arXiv:1410.4447](#)].
- [19] D. Adams et al., *Towards an Understanding of the Correlations in Jet Substructure*, *Eur. Phys. J. C* **75** (2015), no. 9 409, [[arXiv:1504.00679](#)].
- [20] A. J. Larkoski, I. Moult, and B. Nachman, *Jet Substructure at the Large Hadron Collider: A Review of Recent Advances in Theory and Machine Learning*, *Phys. Rept.* **841** (2020) 1–63, [[arXiv:1709.04464](#)].
- [21] A. Butter et al., *The Machine Learning landscape of top taggers*, *SciPost Phys.* **7** (2019) 014, [[arXiv:1902.09914](#)].
- [22] L. Benato, P. L. S. Connor, G. Kasieczka, D. Krücker, and M. Meyer, *Teaching machine learning with an application in collider particle physics*, *JINST* **15** (2020), no. 09 C09011.
- [23] O. Fedkevych, C. K. Khosa, S. Marzani, and F. Sforza, *Identification of b jets using QCD-inspired observables*, *Phys. Rev. D* **107** (2023), no. 3 034032, [[arXiv:2202.05082](#)].
- [24] S. Caletti, O. Fedkevych, S. Marzani, and D. Reichelt, *Tagging the initial-state gluon*, *Eur. Phys. J. C* **81** (2021), no. 9 844, [[arXiv:2108.10024](#)].
- [25] F. A. Dreyer, G. Soyez, and A. Takacs, *Quarks and gluons in the Lund plane*, *JHEP* **08** (2022) 177, [[arXiv:2112.09140](#)].
- [26] L. Cavallini, A. Coccaro, C. K. Khosa, G. Manco, S. Marzani, F. Parodi, D. Rebutti, A. Rescia, and G. Stagnitto, *Tagging the Higgs boson decay to bottom quarks with colour-sensitive observables and the Lund jet plane*, *Eur. Phys. J. C* **82** (2022), no. 5 493, [[arXiv:2112.09650](#)].
- [27] C. K. Khosa and S. Marzani, *Higgs boson tagging with the Lund jet plane*, *Phys. Rev. D* **104** (2021), no. 5 055043, [[arXiv:2105.03989](#)].
- [28] F. A. Dreyer and H. Qu, *Jet tagging in the Lund plane with graph networks*, *JHEP* **03** (2021) 052, [[arXiv:2012.08526](#)].
- [29] P. Baroň, M. H. Seymour, and A. Siódmok, *Novel approach to measure quark/gluon jets at the LHC*, *Eur. Phys. J. C* **84** (2024), no. 1 28, [[arXiv:2307.15378](#)].
- [30] K. Lapidus and M. H. Oliver, *Hard Substructure of Quenched Jets: a Monte Carlo Study*, [[arXiv:1711.00897](#)].
- [31] K. C. Zapp, *Jet energy loss and equilibration*, *Nucl. Phys. A* **967** (2017) 81–88.
- [32] K. Tywoniuk and Y. Mehtar-Tani, *Measuring medium-induced gluons via jet grooming*, *Nucl. Phys. A* **967** (2017) 520–523.
- [33] J. Casalderrey-Solana, Y. Mehtar-Tani, C. A. Salgado, and K. Tywoniuk, *Probing jet decoherence in heavy ion collisions*, *Nucl. Phys. A* **967** (2017) 564–567.

- [34] J. Casalderrey-Solana, G. Milhano, D. Pablos, and K. Rajagopal, *Modification of Jet Substructure in Heavy Ion Collisions as a Probe of the Resolution Length of Quark-Gluon Plasma*, *JHEP* **01** (2020) 044, [[arXiv:1907.11248](#)].
- [35] M. L. Mangano and B. Nachman, *Observables for possible QGP signatures in central pp collisions*, *Eur. Phys. J. C* **78** (2018), no. 4 343, [[arXiv:1708.08369](#)].
- [36] G.-Y. Qin, *Modification of jet rate, shape and structure: model and phenomenology*, *Nucl. Part. Phys. Proc.* **289-290** (2017) 47–52.
- [37] G. Milhano, U. A. Wiedemann, and K. C. Zapp, *Sensitivity of jet substructure to jet-induced medium response*, *Phys. Lett. B* **779** (2018) 409–413, [[arXiv:1707.04142](#)].
- [38] N.-B. Chang, S. Cao, and G.-Y. Qin, *Probing medium-induced jet splitting and energy loss in heavy-ion collisions*, *Phys. Lett. B* **781** (2018) 423–432, [[arXiv:1707.03767](#)].
- [39] R. Kunnawalkam Elayavalli and K. C. Zapp, *Medium response in JEWEL and its impact on jet shape observables in heavy ion collisions*, *JHEP* **07** (2017) 141, [[arXiv:1707.01539](#)].
- [40] **ALICE** Collaboration, S. Acharya et al., *First measurement of jet mass in Pb–Pb and p–Pb collisions at the LHC*, *Phys. Lett. B* **776** (2018) 249–264, [[arXiv:1702.00804](#)].
- [41] **ALICE** Collaboration, S. Acharya et al., *Medium modification of the shape of small-radius jets in central Pb-Pb collisions at $\sqrt{s_{NN}} = 2.76$ TeV*, *JHEP* **10** (2018) 139, [[arXiv:1807.06854](#)].
- [42] **CMS** Collaboration, V. Khachatryan et al., *Dijet Azimuthal Decorrelations in pp Collisions at $\sqrt{s} = 7$ TeV*, *Phys. Rev. Lett.* **106** (2011) 122003, [[arXiv:1101.5029](#)].
- [43] **CMS** Collaboration, S. Chatrchyan et al., *Modification of Jet Shapes in PbPb Collisions at $\sqrt{s_{NN}} = 2.76$ TeV*, *Phys. Lett. B* **730** (2014) 243–263, [[arXiv:1310.0878](#)].
- [44] **CMS** Collaboration, S. Chatrchyan et al., *Studies of Jet Mass in Dijet and W/Z + Jet Events*, *JHEP* **05** (2013) 090, [[arXiv:1303.4811](#)].
- [45] **CMS** Collaboration, S. Chatrchyan et al., *Event Shapes and Azimuthal Correlations in Z + Jets Events in pp Collisions at $\sqrt{s} = 7$ TeV*, *Phys. Lett. B* **722** (2013) 238–261, [[arXiv:1301.1646](#)].
- [46] **CMS** Collaboration, S. Chatrchyan et al., *Studies of dijet transverse momentum balance and pseudorapidity distributions in pPb collisions at $\sqrt{s_{NN}} = 5.02$ TeV*, *Eur. Phys. J. C* **74** (2014), no. 7 2951, [[arXiv:1401.4433](#)].
- [47] **CMS** Collaboration, V. Khachatryan et al., *Measurements of differential production cross sections for a Z boson in association with jets in pp collisions at $\sqrt{s} = 8$ TeV*, *JHEP* **04** (2017) 022, [[arXiv:1611.03844](#)].
- [48] **CMS** Collaboration, A. M. Sirunyan et al., *Study of Jet Quenching with Z + jet Correlations in Pb-Pb and pp Collisions at $\sqrt{s_{NN}} = 5.02$ TeV*, *Phys. Rev. Lett.* **119** (2017), no. 8 082301, [[arXiv:1702.01060](#)].
- [49] **CMS** Collaboration, A. M. Sirunyan et al., *Measurement of the jet mass in highly boosted $t\bar{t}$ events from pp collisions at $\sqrt{s} = 8$ TeV*, *Eur. Phys. J. C* **77** (2017), no. 7 467, [[arXiv:1703.06330](#)].
- [50] **CMS** Collaboration, A. M. Sirunyan et al., *Observation of Medium-Induced Modifications of Jet Fragmentation in Pb-Pb Collisions at $\sqrt{s_{NN}} = 5.02$ TeV Using Isolated Photon-Tagged Jets*, *Phys. Rev. Lett.* **121** (2018), no. 24 242301, [[arXiv:1801.04895](#)].

- [51] **CMS** Collaboration, A. M. Sirunyan et al., *Measurement of the groomed jet mass in PbPb and pp collisions at $\sqrt{s_{\text{NN}}} = 5.02$ TeV*, *JHEP* **10** (2018) 161, [[arXiv:1805.05145](#)].
- [52] **CMS** Collaboration, A. M. Sirunyan et al., *Measurements of the differential jet cross section as a function of the jet mass in dijet events from proton-proton collisions at $\sqrt{s} = 13$ TeV*, *JHEP* **11** (2018) 113, [[arXiv:1807.05974](#)].
- [53] **CMS** Collaboration, A. M. Sirunyan et al., *Measurement of jet substructure observables in $t\bar{t}$ events from proton-proton collisions at $\sqrt{s} = 13$ TeV*, *Phys. Rev. D* **98** (2018), no. 9 092014, [[arXiv:1808.07340](#)].
- [54] **CMS** Collaboration, A. M. Sirunyan et al., *Measurement of the Jet Mass Distribution and Top Quark Mass in Hadronic Decays of Boosted Top Quarks in pp Collisions at $\sqrt{s} = 13$ TeV*, *Phys. Rev. Lett.* **124** (2020), no. 20 202001, [[arXiv:1911.03800](#)].
- [55] **ATLAS** Collaboration, G. Aad et al., *Measurement of Dijet Azimuthal Decorrelations in pp Collisions at $\sqrt{s} = 7$ TeV*, *Phys. Rev. Lett.* **106** (2011) 172002, [[arXiv:1102.2696](#)].
- [56] **ATLAS** Collaboration, G. Aad et al., *ATLAS Measurements of the Properties of Jets for Boosted Particle Searches*, *Phys. Rev. D* **86** (2012) 072006, [[arXiv:1206.5369](#)].
- [57] **ATLAS** Collaboration, G. Aad et al., *Jet mass and substructure of inclusive jets in $\sqrt{s} = 7$ TeV pp collisions with the ATLAS experiment*, *JHEP* **05** (2012) 128, [[arXiv:1203.4606](#)].
- [58] **ATLAS** Collaboration, G. Aad et al., *Measurements of jet vetoes and azimuthal decorrelations in dijet events produced in pp collisions at $\sqrt{s} = 7$ TeV using the ATLAS detector*, *Eur. Phys. J. C* **74** (2014), no. 11 3117, [[arXiv:1407.5756](#)].
- [59] **ATLAS** Collaboration, M. Aaboud et al., *Measurement of jet fragmentation in Pb+Pb and pp collisions at $\sqrt{s_{\text{NN}}} = 2.76$ TeV with the ATLAS detector at the LHC*, *Eur. Phys. J. C* **77** (2017), no. 6 379, [[arXiv:1702.00674](#)].
- [60] **ATLAS** Collaboration, M. Aaboud et al., *Measurement of the Soft-Drop Jet Mass in pp Collisions at $\sqrt{s} = 13$ TeV with the ATLAS Detector*, *Phys. Rev. Lett.* **121** (2018), no. 9 092001, [[arXiv:1711.08341](#)].
- [61] **ATLAS** Collaboration, M. Aaboud et al., *Measurement of the cross section for isolated-photon plus jet production in pp collisions at $\sqrt{s} = 13$ TeV using the ATLAS detector*, *Phys. Lett. B* **780** (2018) 578–602, [[arXiv:1801.00112](#)].
- [62] **ATLAS** Collaboration, *Measurement of $R = 0.4$ jet mass in Pb+Pb and pp collisions at $\sqrt{s_{\text{NN}}} = 5.02$ TeV with the ATLAS detector*, .
- [63] **ATLAS** Collaboration, G. Aad et al., *Measurement of the jet mass in high transverse momentum $Z(\rightarrow b\bar{b})\gamma$ production at $\sqrt{s} = 13$ TeV using the ATLAS detector*, *Phys. Lett. B* **812** (2021) 135991, [[arXiv:1907.07093](#)].
- [64] **ATLAS** Collaboration, G. Aad et al., *Measurement of soft-drop jet observables in pp collisions with the ATLAS detector at $\sqrt{s} = 13$ TeV*, *Phys. Rev. D* **101** (2020), no. 5 052007, [[arXiv:1912.09837](#)].
- [65] **STAR** Collaboration, K. Kauder, *Measurement of the Shared Momentum Fraction z_g using Jet Reconstruction in p+p and Au+Au Collisions with STAR*, *Nucl. Phys. A* **967** (2017) 516–519, [[arXiv:1704.03046](#)].
- [66] **STAR** Collaboration, J. Adam et al., *Measurement of groomed jet substructure observables in p+p collisions at $\sqrt{s} = 200$ GeV with STAR*, *Phys. Lett. B* **811** (2020) 135846, [[arXiv:2003.02114](#)].

- [67] **STAR** Collaboration, M. Abdallah et al., *Invariant Jet Mass Measurements in pp Collisions at $\sqrt{s} = 200$ GeV at RHIC*, *Phys. Rev. D* **104** (2021), no. 5 052007, [[arXiv:2103.13286](#)].
- [68] M. Connors, C. Nattrass, R. Reed, and S. Salur, *Jet measurements in heavy ion physics*, *Rev. Mod. Phys.* **90** (2018) 025005, [[arXiv:1705.01974](#)].
- [69] A. Moraes, C. Buttar, and I. Dawson, *Prediction for minimum bias and the underlying event at LHC energies*, *Eur. Phys. J. C* **50** (2007) 435–466.
- [70] C. Bierlich et al., *A comprehensive guide to the physics and usage of PYTHIA 8.3*, *SciPost Phys. Codeb.* **2022** (2022) 8, [[arXiv:2203.11601](#)].
- [71] T. Sjostrand, S. Mrenna, and P. Z. Skands, *PYTHIA 6.4 Physics and Manual*, *JHEP* **05** (2006) 026, [[hep-ph/0603175](#)].
- [72] J. Bellm et al., *Herwig 7.2 release note*, *Eur. Phys. J. C* **80** (2020), no. 5 452, [[arXiv:1912.06509](#)].
- [73] G. Corcella, I. G. Knowles, G. Marchesini, S. Moretti, K. Odagiri, P. Richardson, M. H. Seymour, and B. R. Webber, *HERWIG 6: An Event generator for hadron emission reactions with interfering gluons (including supersymmetric processes)*, *JHEP* **01** (2001) 010, [[hep-ph/0011363](#)].
- [74] **Sherpa** Collaboration, E. Bothmann et al., *Event Generation with Sherpa 2.2*, *SciPost Phys.* **7** (2019), no. 3 034, [[arXiv:1905.09127](#)].
- [75] T. Gleisberg, S. Hoeche, F. Krauss, M. Schonherr, S. Schumann, F. Siegert, and J. Winter, *Event generation with SHERPA 1.1*, *JHEP* **02** (2009) 007, [[arXiv:0811.4622](#)].
- [76] M. R. Aguilar, Z. Chang, R. K. Elayavalli, R. Fatemi, Y. He, Y. Ji, D. Kalinkin, M. Kelsey, I. Mooney, and V. Verkest, *pythia8 underlying event tune for RHIC energies*, *Phys. Rev. D* **105** (2022), no. 1 016011, [[arXiv:2110.09447](#)].
- [77] D. Reichelt, S. Caletti, O. Fedkevych, S. Marzani, S. Schumann, and G. Soyez, *Phenomenology of jet angularities at the LHC*, *JHEP* **03** (2022) 131, [[arXiv:2112.09545](#)].
- [78] C. F. Berger, T. Kucs, and G. F. Sterman, *Event shape / energy flow correlations*, *Phys. Rev. D* **68** (2003) 014012, [[hep-ph/0303051](#)].
- [79] L. G. Almeida, S. J. Lee, G. Perez, G. F. Sterman, I. Sung, and J. Virzi, *Substructure of high- p_T Jets at the LHC*, *Phys. Rev. D* **79** (2009) 074017, [[arXiv:0807.0234](#)].
- [80] A. J. Larkoski, J. Thaler, and W. J. Waalewijn, *Gaining (Mutual) Information about Quark/Gluon Discrimination*, *JHEP* **11** (2014) 129, [[arXiv:1408.3122](#)].
- [81] **CDF** Collaboration, T. Aaltonen et al., *Study of Substructure of High Transverse Momentum Jets Produced in Proton-Antiproton Collisions at $\sqrt{s} = 1.96$ TeV*, *Phys. Rev. D* **85** (2012) 091101, [[arXiv:1106.5952](#)].
- [82] S. Marzani, G. Soyez, and M. Spannowsky, *Looking inside jets: an introduction to jet substructure and boosted-object phenomenology*, vol. 958. Springer, 2019.
- [83] S. Caletti, O. Fedkevych, S. Marzani, D. Reichelt, S. Schumann, G. Soyez, and V. Theeuwes, *Jet angularities in Z+jet production at the LHC*, *JHEP* **07** (2021) 076, [[arXiv:2104.06920](#)].
- [84] Z.-B. Kang, K. Lee, and F. Ringer, *Jet angularity measurements for single inclusive jet production*, *JHEP* **04** (2018) 110, [[arXiv:1801.00790](#)].

- [85] Z.-B. Kang, K. Lee, X. Liu, and F. Ringer, *Soft drop groomed jet angularities at the LHC*, *Phys. Lett. B* **793** (2019) 41–47, [[arXiv:1811.06983](#)].
- [86] L. G. Almeida, S. D. Ellis, C. Lee, G. Sterman, I. Sung, and J. R. Walsh, *Comparing and counting logs in direct and effective methods of QCD resummation*, *JHEP* **04** (2014) 174, [[arXiv:1401.4460](#)].
- [87] M. Dasgupta, B. K. El-Menoufi, and J. Helliwell, *QCD resummation for groomed jet observables at NNLL+NLO*, *JHEP* **01** (2023) 045, [[arXiv:2211.03820](#)].
- [88] A. Budhraj, R. Sharma, and B. Singh, *Medium modifications to jet angularities using SCET with Glauber gluons*, [arXiv:2305.10237](#).
- [89] E. Gerwick, S. Hoeche, S. Marzani, and S. Schumann, *Soft evolution of multi-jet final states*, *JHEP* **02** (2015) 106, [[arXiv:1411.7325](#)].
- [90] N. Baberuxki, C. T. Preuss, D. Reichelt, and S. Schumann, *Resummed predictions for jet-resolution scales in multijet production in e^+e^- annihilation*, *JHEP* **04** (2020) 112, [[arXiv:1912.09396](#)].
- [91] sPHENIX Collaboration, H. Okawa, *Status and Performance of sPHENIX Experiment*, *EPJ Web Conf.* **276** (2023) 05004.
- [92] N. Armesto, L. Cunqueiro, and C. A. Salgado, *Q-PYTHIA: A Medium-modified implementation of final state radiation*, *Eur. Phys. J. C* **63** (2009) 679–690, [[arXiv:0907.1014](#)].
- [93] K. C. Zapp, *JEWEL 2.0.0: directions for use*, *Eur. Phys. J. C* **74** (2014), no. 2 2762, [[arXiv:1311.0048](#)].
- [94] M. Cacciari, G. P. Salam, and G. Soyez, *FastJet User Manual*, *Eur. Phys. J. C* **72** (2012) 1896, [[arXiv:1111.6097](#)].
- [95] M. Cacciari, G. P. Salam, and G. Soyez, *The anti- k_t jet clustering algorithm*, *JHEP* **04** (2008) 063, [[arXiv:0802.1189](#)].
- [96] J. Currie, A. Gehrmann-De Ridder, T. Gehrmann, E. W. N. Glover, A. Huss, and J. a. Pires, *Infrared sensitivity of single jet inclusive production at hadron colliders*, *JHEP* **10** (2018) 155, [[arXiv:1807.03692](#)].
- [97] J. R. Andersen et al., *Les Houches 2015: Physics at TeV Colliders Standard Model Working Group Report*, in *9th Les Houches Workshop on Physics at TeV Colliders*, 5, 2016. [[arXiv:1605.04692](#)].
- [98] A. Banfi, G. P. Salam, and G. Zanderighi, *Principles of general final-state resummation and automated implementation*, *JHEP* **03** (2005) 073, [[hep-ph/0407286](#)].
- [99] A. J. Larkoski, G. P. Salam, and J. Thaler, *Energy Correlation Functions for Jet Substructure*, *JHEP* **06** (2013) 108, [[arXiv:1305.0007](#)].
- [100] A. J. Larkoski, D. Neill, and J. Thaler, *Jet Shapes with the Broadening Axis*, *JHEP* **04** (2014) 017, [[arXiv:1401.2158](#)].
- [101] S. Marzani, L. Schunk, and G. Soyez, *A study of jet mass distributions with grooming*, *JHEP* **07** (2017) 132, [[arXiv:1704.02210](#)].
- [102] A. J. Larkoski, S. Marzani, G. Soyez, and J. Thaler, *Soft Drop*, *JHEP* **05** (2014) 146, [[arXiv:1402.2657](#)].

- [103] Y. L. Dokshitzer, G. D. Leder, S. Moretti, and B. R. Webber, *Better jet clustering algorithms*, *JHEP* **08** (1997) 001, [[hep-ph/9707323](#)].
- [104] M. Wobisch and T. Wengler, *Hadronization corrections to jet cross-sections in deep inelastic scattering*, in *Workshop on Monte Carlo Generators for HERA Physics (Plenary Starting Meeting)*, pp. 270–279, 4, 1998. [hep-ph/9907280](#).
- [105] A. Buckley, J. Butterworth, D. Grellscheid, H. Hoeth, L. Lonnblad, J. Monk, H. Schulz, and F. Siegert, *Rivet user manual*, *Comput. Phys. Commun.* **184** (2013) 2803–2819, [[arXiv:1003.0694](#)].
- [106] C. Bierlich et al., *Robust Independent Validation of Experiment and Theory: Rivet version 3*, *SciPost Phys.* **8** (2020) 026, [[arXiv:1912.05451](#)].
- [107] J. D. Hunter, *Matplotlib: A 2D Graphics Environment*, *Comput. Sci. Eng.* **9** (2007), no. 3 90–95.
- [108] A. Banfi, G. P. Salam, and G. Zanderighi, *Phenomenology of event shapes at hadron colliders*, *JHEP* **06** (2010) 038, [[arXiv:1001.4082](#)].
- [109] S. Marzani, D. Reichelt, S. Schumann, G. Soyez, and V. Theeuwes, *Fitting the Strong Coupling Constant with Soft-Drop Thrust*, *JHEP* **11** (2019) 179, [[arXiv:1906.10504](#)].
- [110] J. Baron, D. Reichelt, S. Schumann, N. Schwanemann, and V. Theeuwes, *Soft-drop grooming for hadronic event shapes*, *JHEP* **07** (2021) 142, [[arXiv:2012.09574](#)].
- [111] M. Knobbe, D. Reichelt, and S. Schumann, *(N)NLO+NLL’ accurate predictions for plain and groomed 1-jettiness in neutral current DIS*, *JHEP* **09** (2023) 194, [[arXiv:2306.17736](#)].
- [112] **H1** Collaboration, V. Andreev et al., *Measurement of the 1-jettiness event shape observable in deep-inelastic electron-proton scattering at HERA*, [arXiv:2403.10109](#).
- [113] **H1** Collaboration, V. Andreev et al., *Measurement of groomed event shape observables in deep-inelastic electron-proton scattering at HERA*, [arXiv:2403.10134](#).
- [114] A. Gehrmann-De Ridder, C. T. Preuss, D. Reichelt, and S. Schumann, *NLO+NLL’ accurate predictions for three-jet event shapes in hadronic Higgs decays*, [arXiv:2403.06929](#).
- [115] M. Dasgupta and G. P. Salam, *Resummation of nonglobal QCD observables*, *Phys. Lett. B* **512** (2001) 323–330, [[hep-ph/0104277](#)].
- [116] M. Dasgupta, K. Khelifa-Kerfa, S. Marzani, and M. Spannowsky, *On jet mass distributions in Z+jet and dijet processes at the LHC*, *JHEP* **10** (2012) 126, [[arXiv:1207.1640](#)].
- [117] M. Dasgupta, A. Fregoso, S. Marzani, and G. P. Salam, *Towards an understanding of jet substructure*, *JHEP* **09** (2013) 029, [[arXiv:1307.0007](#)].
- [118] T. Gleisberg and S. Hoeche, *Comix, a new matrix element generator*, *JHEP* **12** (2008) 039, [[arXiv:0808.3674](#)].
- [119] T. Gleisberg and F. Krauss, *Automating dipole subtraction for QCD NLO calculations*, *Eur. Phys. J. C* **53** (2008) 501–523, [[arXiv:0709.2881](#)].
- [120] S. Actis, A. Denner, L. Hofer, J.-N. Lang, A. Scharf, and S. Uccirati, *RECOLA: REcursive Computation of One-Loop Amplitudes*, *Comput. Phys. Commun.* **214** (2017) 140–173, [[arXiv:1605.01090](#)].
- [121] B. Biedermann, S. Bräuer, A. Denner, M. Pellen, S. Schumann, and J. M. Thompson, *Automation of NLO QCD and EW corrections with Sherpa and Recola*, *Eur. Phys. J. C* **77** (2017) 492, [[arXiv:1704.05783](#)].

- [122] F. Cascioli, P. Maierhofer, and S. Pozzorini, *Scattering Amplitudes with Open Loops*, *Phys. Rev. Lett.* **108** (2012) 111601, [[arXiv:1111.5206](#)].
- [123] S. Caletti, A. J. Larkoski, S. Marzani, and D. Reichelt, *A fragmentation approach to jet flavor*, *JHEP* **10** (2022) 158, [[arXiv:2205.01117](#)].
- [124] S. Caletti, A. J. Larkoski, S. Marzani, and D. Reichelt, *Practical jet flavour through NNLO*, *Eur. Phys. J. C* **82** (2022), no. 7 632, [[arXiv:2205.01109](#)].
- [125] M. Czakon, A. Mitov, and R. Poncelet, *Infrared-safe flavoured anti- k_T jets*, *JHEP* **04** (2023) 138, [[arXiv:2205.11879](#)].
- [126] R. Gauld, A. Huss, and G. Stagnitto, *Flavor Identification of Reconstructed Hadronic Jets*, *Phys. Rev. Lett.* **130** (2023), no. 16 161901, [[arXiv:2208.11138](#)].
- [127] F. Caola, R. Grabarczyk, M. L. Hutt, G. P. Salam, L. Scyboz, and J. Thaler, *Flavored jets with exact anti- k_T kinematics and tests of infrared and collinear safety*, *Phys. Rev. D* **108** (2023), no. 9 094010, [[arXiv:2306.07314](#)].
- [128] A. Banfi, G. P. Salam, and G. Zanderighi, *Infrared safe definition of jet flavor*, *Eur. Phys. J. C* **47** (2006) 113–124, [[hep-ph/0601139](#)].
- [129] **PDF4LHC Working Group** Collaboration, R. D. Ball et al., *The PDF4LHC21 combination of global PDF fits for the LHC Run III*, *J. Phys. G* **49** (2022), no. 8 080501, [[arXiv:2203.05506](#)].
- [130] A. Buckley, J. Ferrando, S. Lloyd, K. Nordström, B. Page, M. Rüfenacht, M. Schönherr, and G. Watt, *LHAPDF6: parton density access in the LHC precision era*, *Eur. Phys. J. C* **75** (2015) 132, [[arXiv:1412.7420](#)].
- [131] E. Bothmann, M. Schönherr, and S. Schumann, *Reweighting QCD matrix-element and parton-shower calculations*, *Eur. Phys. J. C* **76** (2016), no. 11 590, [[arXiv:1606.08753](#)].
- [132] A. Buckley et al., *General-purpose event generators for LHC physics*, *Phys. Rept.* **504** (2011) 145–233, [[arXiv:1101.2599](#)].
- [133] J. M. Campbell et al., *Event Generators for High-Energy Physics Experiments*, in *Snowmass 2021*, 3, 2022. [[arXiv:2203.11110](#)].
- [134] A. V. Manohar and M. B. Wise, *Power suppressed corrections to hadronic event shapes*, *Phys. Lett. B* **344** (1995) 407–412, [[hep-ph/9406392](#)].
- [135] Y. L. Dokshitzer and B. R. Webber, *Calculation of power corrections to hadronic event shapes*, *Phys. Lett. B* **352** (1995) 451–455, [[hep-ph/9504219](#)].
- [136] R. Akhoury and V. I. Zakharov, *On the universality of the leading, $1/Q$ power corrections in QCD*, *Phys. Lett. B* **357** (1995) 646–652, [[hep-ph/9504248](#)].
- [137] G. P. Korchemsky and G. F. Sterman, *Universality of infrared renormalons in hadronic cross-sections*, in *30th Rencontres de Moriond: QCD and High-energy Hadronic Interactions*, pp. 383–391, 1995. [[hep-ph/9505391](#)].
- [138] Y. L. Dokshitzer, G. Marchesini, and G. P. Salam, *Revisiting nonperturbative effects in the jet broadenings*, *Eur. Phys. J. direct* **1** (1999), no. 1 3, [[hep-ph/9812487](#)].
- [139] S. Hoeche, F. Krauss, M. Schonherr, and F. Siegert, *QCD matrix elements + parton showers: The NLO case*, *JHEP* **04** (2013) 027, [[arXiv:1207.5030](#)].
- [140] S. Schumann and F. Krauss, *A Parton shower algorithm based on Catani-Seymour dipole factorisation*, *JHEP* **03** (2008) 038, [[arXiv:0709.1027](#)].

- [141] A. Denner, S. Dittmaier, and L. Hofer, *Collier: a fortran-based Complex One-Loop Library in Extended Regularizations*, *Comput. Phys. Commun.* **212** (2017) 220–238, [[arXiv:1604.06792](#)].
- [142] T. Sjostrand and M. van Zijl, *A Multiple Interaction Model for the Event Structure in Hadron Collisions*, *Phys. Rev. D* **36** (1987) 2019.
- [143] G. S. Chahal and F. Krauss, *Cluster Hadronisation in Sherpa*, *SciPost Phys.* **13** (2022), no. 2 019, [[arXiv:2203.11385](#)].
- [144] M. Knobbe, F. Krauss, D. Reichelt, and S. Schumann, *Measuring hadronic Higgs boson branching ratios at future lepton colliders*, *Eur. Phys. J. C* **84** (2024), no. 1 83, [[arXiv:2306.03682](#)].
- [145] T. Sjostrand and P. Z. Skands, *Transverse-momentum-ordered showers and interleaved multiple interactions*, *Eur. Phys. J. C* **39** (2005) 129–154, [[hep-ph/0408302](#)].
- [146] R. Corke and T. Sjostrand, *Interleaved Parton Showers and Tuning Prospects*, *JHEP* **03** (2011) 032, [[arXiv:1011.1759](#)].
- [147] P. Skands, S. Carrazza, and J. Rojo, *Tuning PYTHIA 8.1: the Monash 2013 Tune*, *Eur. Phys. J. C* **74** (2014), no. 8 3024, [[arXiv:1404.5630](#)].
- [148] A. H. Hoang, S. Mantry, A. Pathak, and I. W. Stewart, *Nonperturbative Corrections to Soft Drop Jet Mass*, *JHEP* **12** (2019) 002, [[arXiv:1906.11843](#)].
- [149] A. Pathak, I. W. Stewart, V. Vaidya, and L. Zoppi, *EFT for Soft Drop Double Differential Cross Section*, *JHEP* **04** (2021) 032, [[arXiv:2012.15568](#)].
- [150] T. Sjöstrand, S. Ask, J. R. Christiansen, R. Corke, N. Desai, P. Ilten, S. Mrenna, S. Prestel, C. O. Rasmussen, and P. Z. Skands, *An introduction to PYTHIA 8.2*, *Comput. Phys. Commun.* **191** (2015) 159–177, [[arXiv:1410.3012](#)].
- [151] M. Dasgupta, L. Magnea, and G. P. Salam, *Non-perturbative QCD effects in jets at hadron colliders*, *JHEP* **02** (2008) 055, [[arXiv:0712.3014](#)].
- [152] G. P. Korchemsky and G. F. Sterman, *Power corrections to event shapes and factorization*, *Nucl. Phys. B* **555** (1999) 335–351, [[hep-ph/9902341](#)].
- [153] L. P. Csernai, *Introduction to relativistic heavy ion collisions*. 1994.
- [154] A. Accardi et al., *Hard probes in heavy ion collisions at the LHC: Jet physics*, [[hep-ph/0310274](#)].
- [155] J. D. Bjorken, *Energy Loss of Energetic Partons in Quark - Gluon Plasma: Possible Extinction of High $p(t)$ Jets in Hadron - Hadron Collisions*, .
- [156] M. Gyulassy and M. Plumer, *Jet Quenching in Dense Matter*, *Phys. Lett. B* **243** (1990) 432–438.
- [157] X.-N. Wang and M. Gyulassy, *HIJING: A Monte Carlo model for multiple jet production in $p p$, $p A$ and $A A$ collisions*, *Phys. Rev. D* **44** (1991) 3501–3516.
- [158] X.-N. Wang and M. Gyulassy, *Gluon shadowing and jet quenching in $A + A$ collisions at $s^{*}(1/2) = 200\text{-GeV}$* , *Phys. Rev. Lett.* **68** (1992) 1480–1483.
- [159] M. Gyulassy and X.-n. Wang, *Multiple collisions and induced gluon Bremsstrahlung in QCD*, *Nucl. Phys. B* **420** (1994) 583–614, [[nucl-th/9306003](#)].

- [160] J. Casalderrey-Solana and C. A. Salgado, *Introductory lectures on jet quenching in heavy ion collisions*, *Acta Phys. Polon. B* **38** (2007) 3731–3794, [[arXiv:0712.3443](#)].
- [161] D. d’Enterria, *Jet quenching*, *Landolt-Bornstein* **23** (2010) 471, [[arXiv:0902.2011](#)].
- [162] C. A. Salgado and U. A. Wiedemann, *Medium modification of jet shapes and jet multiplicities*, *Phys. Rev. Lett.* **93** (2004) 042301, [[hep-ph/0310079](#)].
- [163] N. Borghini and U. A. Wiedemann, *Distorting the hump-backed plateau of jets with dense QCD matter*, [hep-ph/0506218](#).
- [164] N. Armesto, L. Cunqueiro, and C. A. Salgado, *Implementation of a medium-modified parton shower algorithm*, *Eur. Phys. J. C* **61** (2009) 775–778, [[arXiv:0809.4433](#)].
- [165] N. Armesto, C. Pajares, and P. Quiroga-Arias, *Medium dependence of multiplicity distributions in MLLA*, *Eur. Phys. J. C* **61** (2009) 779–784, [[arXiv:0809.4428](#)].
- [166] R. Perez Ramos, *Medium-modified average multiplicity and multiplicity fluctuations in jets*, *Eur. Phys. J. C* **62** (2009) 541–545, [[arXiv:0811.2418](#)].
- [167] R. Perez Ramos, *Medium-modified evolution of multiparticle production in jets in heavy-ion collisions*, *J. Phys. G* **36** (2009) 105006, [[arXiv:0811.2934](#)].
- [168] A. Dainese, C. Loizides, and G. Paic, *Leading-particle suppression in high energy nucleus-nucleus collisions*, *Eur. Phys. J. C* **38** (2005) 461–474, [[hep-ph/0406201](#)].
- [169] J. Casalderrey-Solana, D. C. Gulhan, J. G. Milhano, D. Pablos, and K. Rajagopal, *A Hybrid Strong/Weak Coupling Approach to Jet Quenching*, *JHEP* **10** (2014) 019, [[arXiv:1405.3864](#)]. [Erratum: JHEP 09, 175 (2015)].
- [170] J. H. Putschke et al., *The JETSCAPE framework*, [arXiv:1903.07706](#).
- [171] B. Schenke, S. Jeon, and C. Gale, *(3+1)D hydrodynamic simulation of relativistic heavy-ion collisions*, *Phys. Rev. C* **82** (2010) 014903, [[arXiv:1004.1408](#)].
- [172] I. Karpenko, P. Huovinen, and M. Bleicher, *A 3+1 dimensional viscous hydrodynamic code for relativistic heavy ion collisions*, *Comput. Phys. Commun.* **185** (2014) 3016–3027, [[arXiv:1312.4160](#)].
- [173] C. Shen, Z. Qiu, H. Song, J. Bernhard, S. Bass, and U. Heinz, *The iEBE-VISHNU code package for relativistic heavy-ion collisions*, *Comput. Phys. Commun.* **199** (2016) 61–85, [[arXiv:1409.8164](#)].
- [174] D. Bazow, U. W. Heinz, and M. Strickland, *Massively parallel simulations of relativistic fluid dynamics on graphics processing units with CUDA*, *Comput. Phys. Commun.* **225** (2018) 92–113, [[arXiv:1608.06577](#)].
- [175] L.-G. Pang, H. Petersen, and X.-N. Wang, *Pseudorapidity distribution and decorrelation of anisotropic flow within the open-computing-language implementation CLVisc hydrodynamics*, *Phys. Rev. C* **97** (2018), no. 6 064918, [[arXiv:1802.04449](#)].
- [176] G. Altarelli and G. Parisi, *Asymptotic Freedom in Parton Language*, *Nucl. Phys. B* **126** (1977) 298–318.
- [177] R. Baier, Y. L. Dokshitzer, A. H. Mueller, S. Peigne, and D. Schiff, *Radiative energy loss of high-energy quarks and gluons in a finite volume quark - gluon plasma*, *Nucl. Phys. B* **483** (1997) 291–320, [[hep-ph/9607355](#)].

- [178] R. Baier, Y. L. Dokshitzer, A. H. Mueller, S. Peigne, and D. Schiff, *Radiative energy loss and $p(T)$ broadening of high-energy partons in nuclei*, *Nucl. Phys. B* **484** (1997) 265–282, [[hep-ph/9608322](#)].
- [179] B. G. Zakharov, *Fully quantum treatment of the Landau-Pomeranchuk-Migdal effect in QED and QCD*, *JETP Lett.* **63** (1996) 952–957, [[hep-ph/9607440](#)].
- [180] B. G. Zakharov, *Radiative energy loss of high-energy quarks in finite size nuclear matter and quark - gluon plasma*, *JETP Lett.* **65** (1997) 615–620, [[hep-ph/9704255](#)].
- [181] B. G. Zakharov, *Light cone path integral approach to the Landau-Pomeranchuk-Migdal effect*, *Phys. Atom. Nucl.* **61** (1998) 838–854, [[hep-ph/9807540](#)].
- [182] U. A. Wiedemann, *Jet quenching versus jet enhancement: A Quantitative study of the BDMPS-Z gluon radiation spectrum*, *Nucl. Phys. A* **690** (2001) 731–751, [[hep-ph/0008241](#)].
- [183] U. A. Wiedemann, *Gluon radiation off hard quarks in a nuclear environment: Opacity expansion*, *Nucl. Phys. B* **588** (2000) 303–344, [[hep-ph/0005129](#)].
- [184] R. Baier, D. Schiff, and B. G. Zakharov, *Energy loss in perturbative QCD*, *Ann. Rev. Nucl. Part. Sci.* **50** (2000) 37–69, [[hep-ph/0002198](#)].
- [185] C. A. Salgado and U. A. Wiedemann, *A Dynamical scaling law for jet tomography*, *Phys. Rev. Lett.* **89** (2002) 092303, [[hep-ph/0204221](#)].
- [186] M. Gyulassy, I. Vitev, X.-N. Wang, and B.-W. Zhang, *Jet quenching and radiative energy loss in dense nuclear matter*, [nucl-th/0302077](#).
- [187] A. Kovner and U. A. Wiedemann, *Gluon radiation and parton energy loss*, [hep-ph/0304151](#).
- [188] C. A. Salgado and U. A. Wiedemann, *Calculating quenching weights*, *Phys. Rev. D* **68** (2003) 014008, [[hep-ph/0302184](#)].
- [189] K. C. Zapp, J. Stachel, and U. A. Wiedemann, *A local Monte Carlo framework for coherent QCD parton energy loss*, *JHEP* **07** (2011) 118, [[arXiv:1103.6252](#)].
- [190] A. D. Polosa and C. A. Salgado, *Jet Shapes in Opaque Media*, *Phys. Rev. C* **75** (2007) 041901, [[hep-ph/0607295](#)].
- [191] K. C. Zapp, F. Krauss, and U. A. Wiedemann, *A perturbative framework for jet quenching*, *JHEP* **03** (2013) 080, [[arXiv:1212.1599](#)].
- [192] K. C. Zapp, *Geometrical aspects of jet quenching in JEWEL*, *Phys. Lett. B* **735** (2014) 157–163, [[arXiv:1312.5536](#)].
- [193] K. C. Zapp, F. Krauss, and U. A. Wiedemann, *Explaining Jet Quenching with Perturbative QCD Alone*, [arXiv:1111.6838](#).
- [194] K. Zapp, G. Ingelman, J. Rathsmann, J. Stachel, and U. A. Wiedemann, *A Monte Carlo Model for 'Jet Quenching'*, *Eur. Phys. J. C* **60** (2009) 617–632, [[arXiv:0804.3568](#)].
- [195] L. D. Landau and I. Pomeranchuk, *Limits of applicability of the theory of bremsstrahlung electrons and pair production at high-energies*, *Dokl. Akad. Nauk Ser. Fiz.* **92** (1953) 535–536.
- [196] A. B. Migdal, *Bremsstrahlung and pair production in condensed media at high-energies*, *Phys. Rev.* **103** (1956) 1811–1820.
- [197] K. Zapp, J. Stachel, and U. A. Wiedemann, *A Local Monte Carlo implementation of the*

- non-abelian Landau-Pomeranchuk-Migdal effect*, *Phys. Rev. Lett.* **103** (2009) 152302, [[arXiv:0812.3888](#)].
- [198] K. Zapp, G. Ingelman, J. Rathsmann, and J. Stachel, *Jet quenching from soft QCD scattering in the quark-gluon plasma*, *Phys. Lett. B* **637** (2006) 179–184, [[hep-ph/0512300](#)].
- [199] J. D. Bjorken, *Highly Relativistic Nucleus-Nucleus Collisions: The Central Rapidity Region*, *Phys. Rev. D* **27** (1983) 140–151.
- [200] K. J. Eskola, K. Kajantie, and J. Lindfors, *Quark and Gluon Production in High-Energy Nucleus-Nucleus Collisions*, *Nucl. Phys. B* **323** (1989) 37–52.
- [201] **ATLAS** Collaboration, *ATLAS Monte Carlo tunes for MC09*, .
- [202] **CTEQ** Collaboration, H. L. Lai, J. Huston, S. Kuhlmann, J. Morfin, F. I. Olness, J. F. Owens, J. Pumplin, and W. K. Tung, *Global QCD analysis of parton structure of the nucleon: CTEQ5 parton distributions*, *Eur. Phys. J. C* **12** (2000) 375–392, [[hep-ph/9903282](#)].
- [203] S. Dulat, T.-J. Hou, J. Gao, M. Guzzi, J. Huston, P. Nadolsky, J. Pumplin, C. Schmidt, D. Stump, and C. P. Yuan, *New parton distribution functions from a global analysis of quantum chromodynamics*, *Phys. Rev. D* **93** (2016), no. 3 033006, [[arXiv:1506.07443](#)].
- [204] I. M. Dremin, G. K. Eyyubova, V. L. Korotkikh, and L. I. Sarycheva, *Two-dimensional discrete wavelet analysis of multiparticle event topology in heavy ion collisions*, *Indian J. Phys.* **85** (2011) 39–44, [[arXiv:0711.1657](#)].
- [205] J. G. Milhano and K. Zapp, *Improved background subtraction and a fresh look at jet sub-structure in JEWEL*, *Eur. Phys. J. C* **82** (2022), no. 11 1010, [[arXiv:2207.14814](#)].
- [206] B. Yan and C. Lee, *Probing light quark Yukawa couplings through angularity distributions in Higgs boson decay*, *JHEP* **03** (2024) 123, [[arXiv:2311.12556](#)].
- [207] A. Ferdinand, K. Lee, and A. Pathak, *Field-theoretic analysis of hadronization using soft drop jet mass*, *Phys. Rev. D* **108** (2023), no. 11 L111501, [[arXiv:2301.03605](#)].